Production / Processing and Metallurgy of Niobium Based Materials

PURIFICATION OF NIOBIUM

K. Schulze*, O. Bach**, D. Lupton** and F. Schreiber**

*Max-Planck-Inst. für Metallforschung
Heisenbergstr. 5
D-7000 Stuttgart 80, West Germany

**W. C. Heraeus GmbH
Heraeusstrasse 12-14
D-6450 Hanau 1, West Germany

Abstract

The current state of the art in producing pure niobium metal is reviewed, dealing firstly with the fundamental aspects of the gas-metal reactions which are employed in the vacuum purification processes. The application of these techniques in the modern industrial production of niobium by electron-beam melting and solid-state sintering is described with examples based on different starting materials. Also discussed are methods that have been used to produce ultra-pure niobium on a laboratory scale, in particular electrolytic refining and electron-beam float zone melting. An essential aspect of the purification of niobium is the analysis of trace impurities. The techniques currently used are outlined. Finally, the main applications of niobium and its alloys are briefly summarized.

Introduction

As is well known, niobium possesses a number of outstanding physical properties. It appears to be a uniquely pure metal which exhibits the properties of a type II superconductor with the highest critical temperature for pure metals, T 9.2K; furthermore, its compounds with A15-phase structure show superconductivity at temperatures up to 24K. Since the first days of the "birth of niobium as ≥ pure metal", several properties have attracted the interest of scientists and engineers, for example, its high melting point of 2741K, the low density in comparison to the other refractory metals, the low neutron cross section for thermal neutrons, its suitable nuclear properties, the ability for hydrogen storage and formation of dielectric oxide layers together with the excellent resistance against chemical reagents and its impressive thermomechanical behavior as a base material for alloys.

In contrast to the very few technical applications developed up to now, the properties of pure niobium have been studied intensively because it serves as a suitable model for bcc metals. Among these properties we find the deformation behavior, recovery and recrystallization processes, high energy neutron monitoring in reactor surveillance programs, electronic structure, electrical and magnetic properties, diffusion of interstitials and radiation damage by elementary particles, surface properties, etc. Nearly all of these properties are strongly dependent on the purity of niobium, and highly sensitive analytical tools have been developed in the last two decades even in the absence of any significant technical application of pure niobium metal.

These intensive efforts directed to the preparation of niobium with the highest purity have resulted in an excellent level of knowledge concerning purification processes on a laboratory scale. Although niobium is generally available with better quality than specified by the producers, the current production processes could be further improved.

Detailed descriptions have been published of the niobium metallurgy, especially of extraction and reduction processes, as well as powder metallurgical fabrication and consolidation by electron-beam melting (EBM) **(1–4).** Therefore, in this contribution the present state of niobium extraction and production is summarized in rough outlines. In deviation from the current literature, Figure **1** shows that during the last decade the niobium production on the basis of pure columbite/tantalite processing was extended by the increasing importance of the pyrochlore branch.

In addition to the classical route, consisting of the carbothermic reduction of Nb_2O_5 and the powder metallurgical purification and consolidation, the aluminothermic reduction of Nb_2O_5 from pyrochlore processing followed by EBM was applied on a larger scale. At first sight, this latter process seems to be the optimum solution. However, the problems of purification involved in the overall process shifted from extraction metallurgy to the metal refining during EBM. This is a direct result of a change from powder metallurgy, where refining of niobium from metallic impurities is less efficient, to the melting technology. The separation of volatile elements, mainly of volatile metals, like Al, from niobium raw material can easily be performed by EBM. But, if starting material with small concentrations of less volatile elements, like Ta and W, is required, these elements must be separated either during extraction or after EBM, e.g. by electrolytic refining.

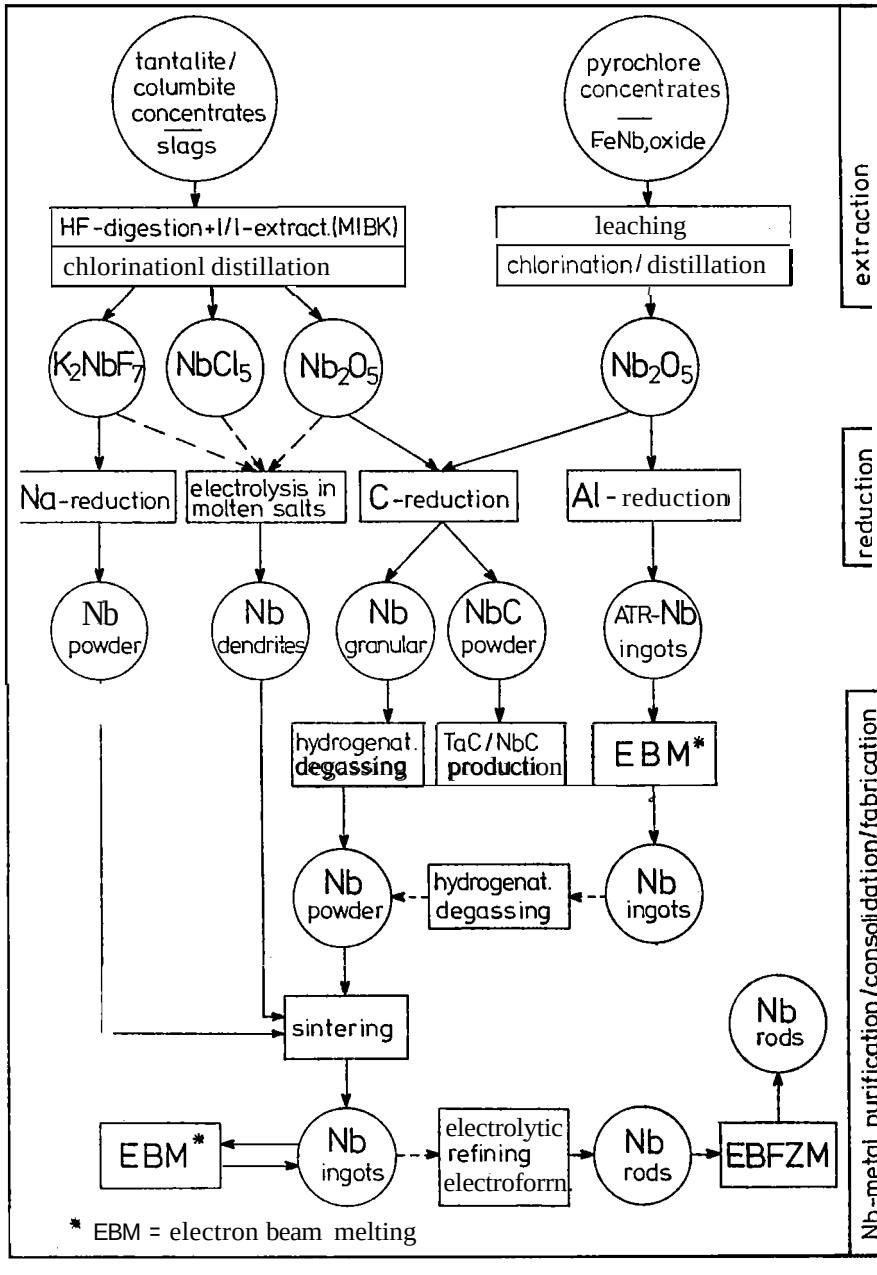

Figure 1. Outline of Niobium Production and Purification Processes.

Similar considerations were applied to the carbothermic reduction route. In this case, metallic impurities which form stable carbides had to be eliminated from the oxide before C-reduction. As was shown, the production of high-grade niobium with small Ta-concentration can be performed via the sodium reduction of purified K_2NbF_7 or via the electrolytic reduction of $NbCl_5$ and/or Nb_2O_5 (5).

An alternative route of niobium fabrication and alloying is powder metallurgy. For special applications it may be convenient to produce powder with high purity hydriding EBM-refined primary metal or scrap. Advanced technologies for the future will most probably be based on the use of niobium with the highest degree of purity. For example, the composition of alloys of superconducting compounds shows that only very low to moderate amounts of substitutional solute elements are allowed and no intentional addition of interstitials should occur. In order to facilitate further developments, high quality material should be made available by the selection of a suitable sequence of purification processes.

A short review of the results of ultrapurification methods for niobium which have been applied in the metallurgical laboratories can give us a guideline for the future development of purification processes on an industrial scale. A brief survey of the efforts directed to preparing high-purity niobium is given in Figure 2, in which the maximum RRR values (residual resistivity ratio) published in each year and the corresponding Ta, W, and interstitial concentrations given in those papers are plotted against the year.

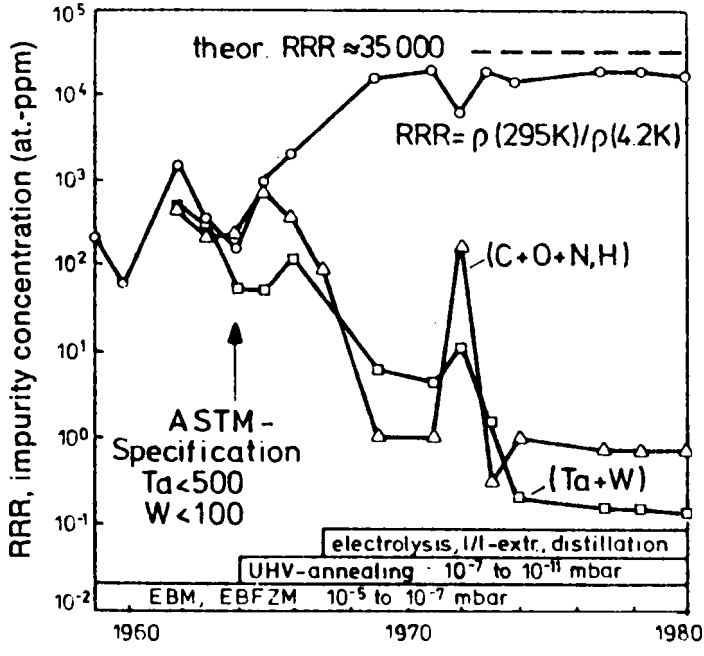

Figure 2. Progress in the Preparation of High-Purity Niobium.

As is well known, the electrical resistivity of metals at low temperatures is an excellent tool to determine impurity concentrations. The residual resistivity at T ≈ 0 is caused mainly by scattering of electrons at impurities. The proportionality constants have been determined for H, C, N and O in Nb as well as for metallic impurities using pure and doped samples: N (5.2), C (4.3), D (4.5), H (0.6), Ta (0.25), Mo (0.21), W (0.4 - 1.1), Zr (1.4 - 0.6), Hf (1.4), Ti (1.4) $\times 10^{-10}$ ohm-cm/ at.ppm. It can be deduced that a concentration equivalent of 1 at. ppm N doubles the resistivity value at 4.2K, whereas 20 at. ppm Ta must be dissolved to get the same effect. For Nb, the ideal RRR equals $\rho(295K) / \rho(4.2K) \approx 3.2 \times 10^{4}$, with $\rho(295K) = 14.58 \times 10^{6}$ and $\rho(4.2K) = 4.5 \times 10^{-10}$ ohm-cm.

The upper curve shows that the RRR values have steadily increased by more than two orders of magnitude in the last two decades and approach the theoretical value.

It is interesting to note that, at the same time, the concentrations of Ta and W and of the interstitially dissolved elements C, O, and N have decreased markedly. Attempts to correlate impurity concentrations with RRR values failed for RRR < 2000 and in one case for R ≈ 6300. For values higher than RRR ≈ 5000 the authors succeeded in calculating the analyzed total impurity concentration from the RRR measurements. This must be credited to improvement of the analytical methods for non-metals as well as to the very high purity of the Nb matrix, free from metallic impurities.

The explanations in the lower part of Figure 2 show the applied purification methods given in the corresponding literature. During the earlier years, electron-beam melting (EBM) and electron-beam float zone melting (EBFZM) were applied exclusively. At that time, neither the thermodynamic and kinetic relations of the reactions between niobium and the residual reactive gases in high vacuum nor the behavior of metallic impurities during EBM or EBFZM were well known. Around 1965, the first fundamental results concerning niobium metal/gas reactions at high temperatures and low pressures ($<10^{-6}$ mbar) were published. At the same time, ultra-high vacuum technology improved and lower gas concentrations resulted. Nevertheless, degassing and decarburization were considered in too simple a way, as will be discussed in more detail later. It can be deduced from the analytical results that volatile metallic impurities did not have any limiting effect on the RRR values between 100 and 500 when EBM or EBFZM methods were used.

In 1964, the first ASTM specification for unalloyed reactor grade Nb was introduced. After this, Ta and W concentrations decreased as a result of improved or new separation methods. Samples prepared by these improved techniques were also used to prepare high-purity niobium. Since 1965 new variants of purification methods have been worked out, leading to further increase in purity. Among these methods, liquid/liquid extraction with methyl-isobutyl-ketone (MIBK) from fluoric aqueous species, distillation of $NbCl_5$ and refining electrolysis in molten fluorides have made essential contributions to the decrease of impurities. The simultaneous application of consecutive refining steps for three different groups of impurities - volatile metallic elements (Al, Fe, Cr, etc.), non-volatile metallic elements with an effective distribution coefficient of $k_{eff} \approx 1$ (Ta,W), and non-metallic elements (H, C, N, O,) - led to a further increase in purity.

Some experimental details of the purification methods illustrated in Figure 2 are shown in Table I. It is evident from the experiments that application of methods for the reduction of Ta and W impurity contents is a prerequisite to preparing high grade starting material. Additionally, it can be stated that the extremely complicated purification procedure (consisting of liquid–liquid extraction and re–extraction of niobium from fluoric water phase with methyl–isobutyl–ketone (MIBK) and chlorination of the oxide under reducing conditions followed by $NbCl_5$ sublimation) did not lead to Ta and W concentrations lower than those achieved by electrolytic refining or reduction processes in molten alkali fluorides or fluoride/chloride mixtures.

Table I. RRR and Purification Steps for High–Purity Niobium.

RRR	Ta–REFINING	EBFZM/O_2*	UHV-ANNEALING PRESSURE/TEMP (K)/TIME
	1/1-MIBK Cl_2/C		
9650	$NbCl_5$-dest.	+/+	3.5×10^{10}/2570/30h
20440	van Arkel Ta=0.8 W=0.7	+/+	4.0×10^{-11}/2570/30h
15080	electrolysis Ta=3.8 W=2.1	-/-	5.0×10^{-9}/2680/ h
20680	electrolysis	-/-	3.0×10^{-10}/2700/ d
5820	elect–red.	+/+	4.0×10^{-10}/2620/41h
14400	electrolysis Ta=0.2 W=0.01	+/+	1.4×10^{-10}/2470/22h
16800	electrolysis Ta=0.1 W=0.005	+/+	1.2×10^{-10}/26600/60h

* Decarburization in O_2: 10^{-5} to 10^{-7} mbar, T ≈ 2200 K

Further purification of niobium with Ta < 10 and W < 2 at. ppm by EBFZM and decarburization in oxygen atmospheres does not give better results, at first sight, than using electolytic refining alone with subsequent degassing. On the other hand, a high RRR value does not guarantee low metallic impurity concentrations. But, significantly, use of reduction electrolysis alone results in a lowered RRR value. Carbon and nitrogen concentrations of electrolytically refined niobium are relatively low (C < 50, N < 60) and oxygen comparatively high (O ≈ 800 at. ppm) due to the solubility of oxygen in alkali fluoride melts. The increased O content enhances decarburization during the degassing step via CO formation, so that a separate decarburization step is unnecessary. The conditions for degassing the samples in ultra–high vacuum are of greater importance: as a consequence of the thermodynamic and kinetic studies of niobium/gas reactions, we know that samples must be annealed at T > 2400K and p < 10^{-9} mbar for several days to achieve a total interstitial concentration < 1 at. ppm and maximum RRR values.

Fundamental Aspects

The great variety of processes occurring during vacuum metallurgical refining of niobium in the solid and liquid state, the different niobium-gas reactions and the evaporation of metallic impurities require distinct theoretical knowledge and technical approaches. Therefore, in this chapter investigations on thermodynamic relations between niobium and non-metallic elements and the strong dependence of equilibrium states, transport by diffusion and reaction rates on pressure, temperature and concentration are briefly summarized. These basic principles must be kept in mind if optimum conditions are to be established during degassing, melting, doping, alloying and heat treatments.

The conditions for optimization of degassing and distillation treatments of niobium are not completely described by the thermodynamic data since they only determine the direction of the reactions occurring under given conditions. The kinetics of the processes are also of great importance. The absolute rate-determining factor is the amount of gas that can be released from the metal surface due to the equilibrium pressure of volatile components. It has been shown that the maximum concentration decrease of a piece of material attainable in a degassing treatment is approximately given by the relation (7).

$$\Delta c \approx 1/2 \cdot p \cdot t/d \qquad (1)$$

where Δc is the concentration change in at. %, p is the equilibrium pressure in mbar, t is the degassing time in s, and d is the thickness of the sample in cm. In Figure 3 the minimum degassing time for the reduction of Δc = 1 at.% of a given impurity is plotted against the equilibrium pressure. It can be deduced that for specimens 10mm thick with high gas content of 1 at.% (e.g., 0.15 wt.% N in Nb at 10^{-5} mbar and 1670K) an effective degassing.

If high equilibrium pressures cannot be reached by using appropriate degassing temperatures, the amount of gas evolved at the surface of the sample is too low to guarantee a reasonable degassing rate. For low concentrations and low equilibrium pressures, UHV-techniques must be applied. Rut in these cases only thin solid specimen or liquid droplets can be degassed. Another rate-limiting factor for the degassing is the diffusion of dissolved atoms to the surface. Because the diffusion coefficients of most metallic impurities in solid niobium at high temperatures are relatively low compared with those of the interstitials, melting operations must be performed. Nevertheless, depletion of metallic elements with high vapor pressures, e.g. Al, Zr, Fe, etc. in surface regions is observed which may be beneficial during refining (e.g., Al-evaporation during sintering of niobium powders) or detrimental during heat treatments (e.g., evaporation of Zr during high temperature annealing of Nb-Zr alloys).

Other effects that can decrease the degassing rate drastically are thermally activated processes on the surface and low rate constants for the formation and evaporation of gas molecules.

Basic considerations about vacuum engineering and the use of vacuum techniques applicable for refining of niobium, sintering and heat treatments are published in the literature (1,2,4).

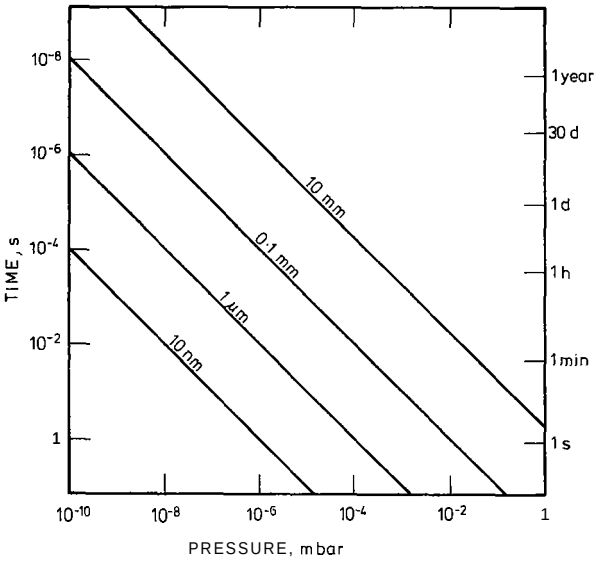

MINIMUM DEGASSING TIME NEEDED IN VACUUM METALLURGICAL TREATMENTS FOR REDUCTION OF IMPURITY CONTENT BY 1 at%

Figure 3. Minimum degassing time needed in vacuum metallurgical treatments for reduction of impurity content by 1 at %.

Niobium–Gas Reactions

One of the most significant characteristics of niobium is its ability to react readily with the gases H_2, N_2, O_2, H_2O, CO, CO_2, C_mH_n and with elementary C. The interaction of niobium with the reactive elements H, N, O and C are not only responsible for undesired changes in physical and mechanical properties (8–10) of the solid metal, but they also play an important role during the fabrication and refining in the solid and liquid states, e.g. during carbothermic reduction of the pentoxide, powder production via the hydriding process, sintering and electron–beam melting (EBM). Moreover, the formation of hydrides, nitrides, oxides and carbides in pure niobium, as well as in niobium–base alloys is of great relevance for its application.

In the following section the niobium–gas reactions are considered from the point of view of purification of the metal during its metallurgical refining by melting and annealing under high vacuum, in an inert gas atmosphere or in reactive gaseous environments for deoxidation or decarburization. The absorption and uptake of H, N, O and C of purified niobium, i.e. the kinetics of surface reactions and diffusion into the bulk at temperatures between 600 and 2000K are thoroughly treated in the contribution by D. Lupton, K. Schulze and F. Aldinger (11). In this paper, the gassing reactions are only taken into account if this is necessary for the understanding of purification, because the highest degree of refining of niobium from gases and carbon which can be achieved must be understood as a change from a given supersaturation of the non–metallic elements in niobium at high temperatures and low partial pressures by decreasing their activity or concentration via lowering the partial pressures of the respective elements in the gas phase with time. The lowest possible concentrations which can be achieved after sufficiently long reaction times are determined by the number of gas molecules striking the surface per unit time at lowest pressure.

From this it can be easily deduced that the time necessary to achieve this final state and the conditions of partial pressures are not only given by the intrinsic factors of the kinetics, i.e. reaction rate, diffusion, dimensions and surface/volume ratio, but also by the practical constraints, e.g. pumping speed, composition of residual gas atmosphere, leakages, etc.

In the solid state, the elements H, N, O and C are dissolved at interstitial sites in niobium (8). The maximum solubility of the interstitials is relatively large at elevated temperatures and decreases with falling and rising temperatures (solvus and solidus lines) so that either precipitation of compounds occurs or the corresponding liquid enriched in gases at equilibrium with the α-solid solution is formed. For both the solid and the liquid, the concentration of the elements at a given partial pressure decreases with increasing temperature.

The mechanics of gassing and degassing reactions between niobium and residual gases in vacuum at high temperatures are schematically shown in Figure 4.

Thermodynamic equilibria are established between H_2 and N_2 and dissolved H and N atoms. For O_2 and H_2O reacting with niobium at temperatures $T > 2000K$ and partial pressures $p < 10^{-4}$ mbar, so-called "steady states" between oxygen uptake and oxide evaporation of NbO or NbO_2 are realized. Reactions between CO and niobium cannot be described by true thermodynamic equilibrium relations because part of the oxygen forms these volatile oxides in an irreversible reaction. Unlike O, C desorbs only through a "mixed" channel in the form of CO. Depending on the relative surface coverages of O and C, either decarburization via CO and formation of NbO (NbO_2) for high O coverages, or only volatile oxide formation for low O coverages may occur. As has been shown, subcritical surface coverages of carbon exist, below which no CO is formed. This is a 'direct result of O desorption through its "own" channel and the reduced probability of a recombination between C and O atoms compared with Nb and O.

Therefore, two ways of decarburization are possible:

1. CO degassing of (C + O) - containing ingots or melts with excess oxygen concentration in the bulk, $c_O > c_C$. This leads to a critical carbon concentration of about 10–40 at.ppm which cannot be removed further due to the strong oxide evaporation.

2. CO degassing by annealing the samples in oxygen atmosphere, e.g. 10^{-5} mbar, to establish an excess surface coverage of O for long periods, during which C can reach the surface by diffusion or hydrodynamic flow.

The reaction kinetics are well established (10). Traces of hydrocarbons which are always present in vacua or inert gases lead to a continuous decomposition at the niobium surface with a steady uptake of C and the liberation of H_2.

In Table 11, calculated interstitial concentrations are compiled, which would be expected after annealing niobium samples under ultra-high vacuum conditions at T = 2500K and a residual pressure $p \approx 10^{-10}$ mbar. These values must be considered as the minimum concentrations which can be achieved after UHV-treatments. In contrast to these results, even for niobium with the

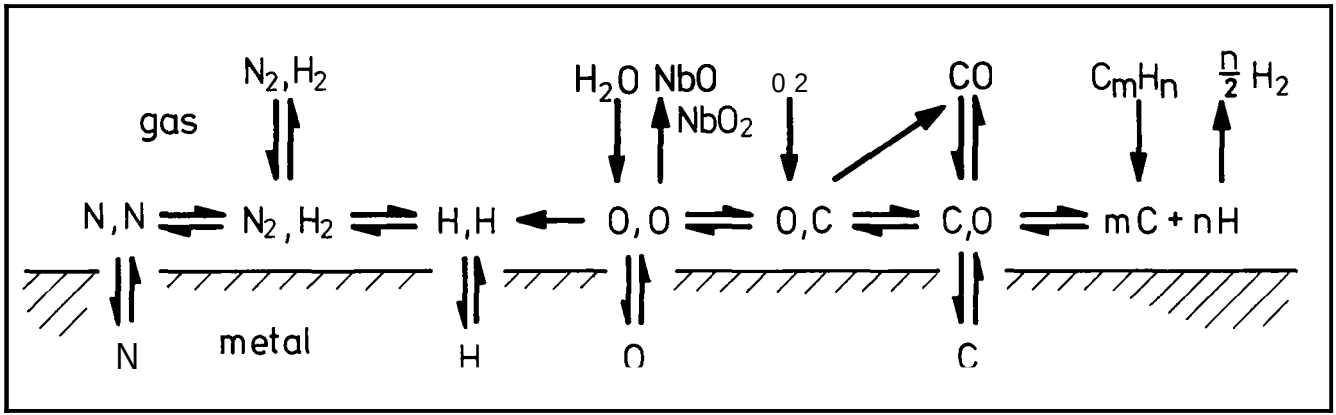

EQUILIBRIUM, STEADY-STATE , DEOXIDATION , CARBURIZATION AND DECARBURIZATION REACTIONS BETWEEN Nb AND H_2 , N_2 , O_2 , H_2O , CO , C_mH_n CONTAINING VACUUM , T > 2000 K.

Figure *4.* **Gas Reactions** with **Niobium.**

highest purity ever produced residual resistivity measurements and gas analysis by a special ultra-high vacuum extraction technique using levitation melting showed that at least 0.1 - 0.5 at. ppm N and C + O were retained in solid solution. The reason for this will be discussed below.

Table II. Calculated Interstitial Concentrations in Niobium After Ultra-High-Vacuum Annealing.

RESIDUAL GASES* Mbar	FINAL CONTENT* at-ppm	REACTIONS
H_2 9.10^{-11}	$\sim 10^{-3}$ H	$H_2 = 2H$
$H_2O \sim 10^{-12}$	$\sim 3.10^{-7}$ O	$H_2O \rightarrow O + H_2 \uparrow$
$O_2 \sim 10^{-12}$		$O_2 \rightarrow 2O$
		$CO = C + O$
$CO - 10^{-11}$	$\sim$ 2.10-6 (C+O)	$O + Nb \rightarrow NbO \downarrow$
$N_2 < 10^{12}$	$- 4.10^{-2}$ N	$N_2 = 2N$
$C_mH_n \sim 10^{-12}$	steady increase	$C_mH_n \rightarrow mC + n2/H_2$

*$P_{CO} > P_{N2}$ T ≈ 2500 K

Thermodynamics and Steady States

For H_2 and N_2, thermodynamic equilibria between the gas phase and the interstitially dissolved H and N atoms are established according to the reactions:

$$H_2\ (g) \rightleftarrows 2\ H\ (\text{in Nb}) \quad \text{and} \tag{1}$$

$$N_2\ (g) \rightleftarrows 2\ N\ (\text{in Nb}). \tag{2}$$

In the Nb-H system between room temperature and 870 K and in the Nb-N system above 1500 K the equilibrium partial pressures of hydrogen and nitrogen over the solid solutions and over the hydride or nitride phases lie in the range covered by vacuum techniques.

The Nb-H phase diagram is shown in Figures 5a and 5b (10,12).

The solubility of H in α-Nb, c_H, obeys the relation

$$\text{H in a-Nb: } \log c_H = 1/2 \log p_{H_2} - 2.91 + 2070/T, \quad (420 < T < 1770K), \tag{3}$$

with p_{H_2} in mbar, T in K and c_H in at.% (13).

The solubility of H in molten niobium is given by the equation

$$\text{H in Nb(l): } \log c_H = 1/2 \log p_{H_2} - 2.00 + 1620/T, \quad (2870 < T < 3100K). \tag{4}$$

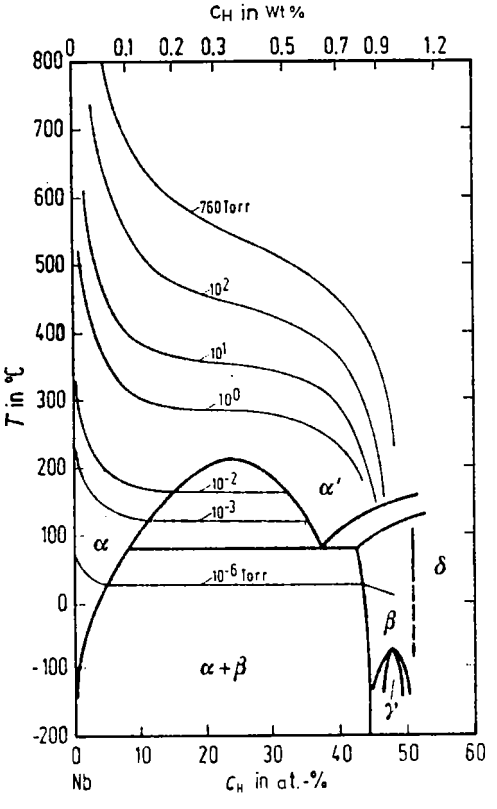

Figure 5(a). Nb-H, T-c Diagram.

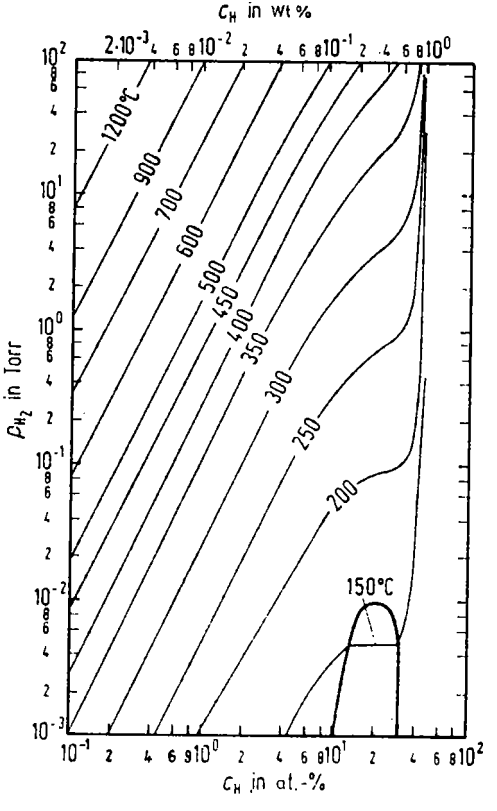

Figure 5(b). Nb-H, p-c Diagram.

At temperatures below 600K oxide-like sorption layers at the niobium surface serve as barriers for the exchange of hydrogen between gas and metal. Therefore, special attention must be paid to the application of the thermodynamic data for Nb-H at lower temperatures or during the course of heating and cooling cycles or solidification.

During the high-temperature annealing or melting of niobium in vacuum, hydrogen is readily picked up at the surface and the rate determining process is the transport in the gas atmosphere or the diffusion in the bulk, depending on the partial pressure and the diffusion paths. Therefore, the lowest possible H-concentration after degassing treatments can easily be calculated from the p-T-c relations. But it must also be taken into account that considerable quantities of H may be picked up during cooling. The rate of H absorption depends on the relative number of O_2 or H_2O and H_2 molecules striking the surface per time unit. In high vacuum equipment ($p \geq 10^{-6}$ mbar) the residual atmosphere mainly consists of H_2O vapor, O_2, N_2 and CO with relatively low H_2 proportions. Here, the surface barriers for H absorption are quickly built up during cooling so that, even for H_2 pressures considerably lower than in UHV systems, comparable H contents are observed. On the other hand, after UHV degassing treatments the surface of niobium specimens is clean without any protecting oxide layer. The residual gas in an UHV chamber at $p < 10^{-7}$ mbar is mainly H_2. When, after annealing or melting at pressures far below 10^{-7} mbar, the vacuum pumps are shut off, H_2 pressure increases for a transient period to 10^{-8} - 10^{-7} mbar. Within a few minutes large quantities of H_2 strike the unprotected surface. At room temperature the equilibrium content of H_2 in niobium is fairly high. For 320K and 10^{-8} mbar, thermodynamic data for H in α-Nb predict about 0.3 - 0.4 at.%. Depending on the surface/volume ratio of the specimen, quantities between several at.ppm and a few hundred at.ppm are dissolved.

The Nb-N phase diagram is shown in Figures 6a and 6b (10, 14).

The p-T-c relationship for N dissolved in niobium at $c < 0.1$ at.-% was partly investigated for the liquid and solid state (15), see Figures 7a and b. From the results shown in Figure 7 the distribution coefficient for N between solid and liquid niobium, $k_o = c_s/c_l$ was calculated as $k = 0.76$.

The solubility of N in α-Nb, c_N, obeys the equation

$$\text{N in } \alpha\text{-Nb: } \log c_N = 1/2 \log p_{N_2} - 3.76 + 9300/T \quad (1770 < T < 2470\text{K}), \tag{5}$$

with p_{N_2} in mbar, T in K and c_N in at.% (10).

The nitrogen solubility in liquid niobium was found to be

$$\text{N in Nb (l): } \log c_N = 1/2 \log p_{N_2} + 0.22 \quad (16) \quad (< 15 \text{ at.\%}, \ T = 2800\text{K}) \tag{6}$$

The pressure-concentration isotherms in Figure 6b show for the region of a-solid solution a slope of 2. Since Sievert's law is obeyed, the N is dissolved in atomic form in the solid solution. The first kink in the

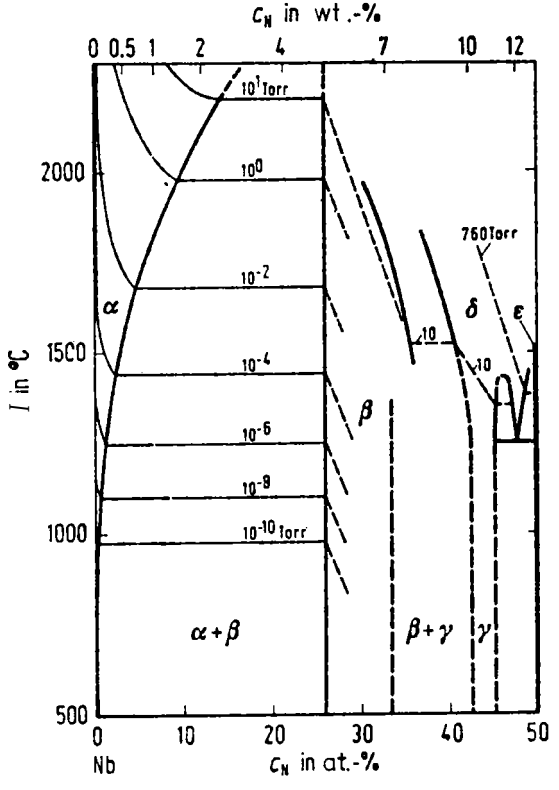

Figure Nb-N System, T-c Diagram.

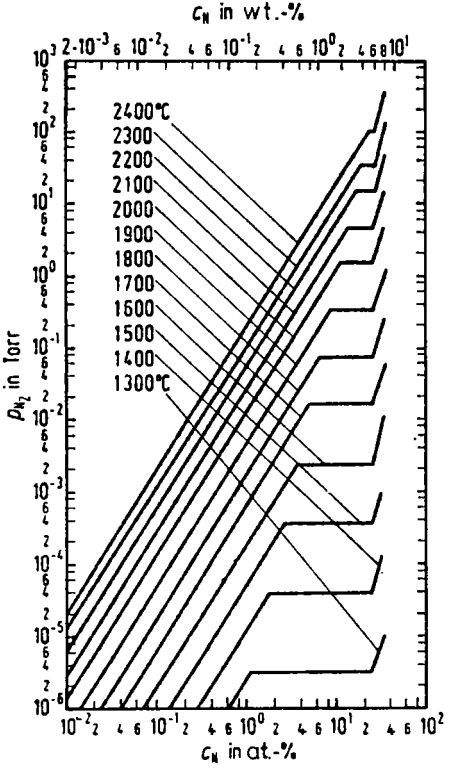

Figure 6(b). Nb-N System, log p-log c Diagram.

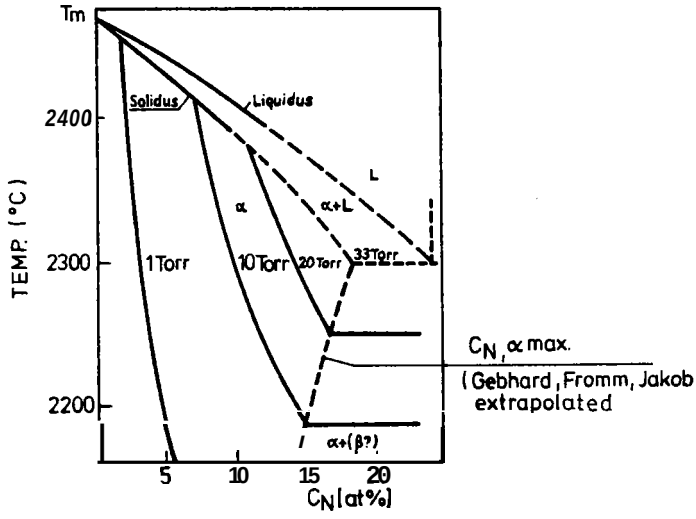

Figure 7(a). Nb-N System, T-c Diagram with Isobars.

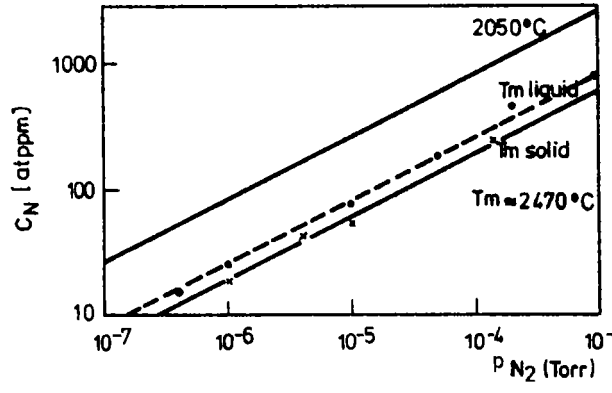

Figure 7(b). Nb-N System, log p-log c Diagram at the Melting Point of Nb.

isotherms gives the concentration at which niobium is saturated with N at the given temperature and the subnitride phase, Nb_2N, is formed. For constant N_2 pressures the N concentration in solid solution decreases with rising temperature.

It is obvious that for all kinds of metallurgical treatments, especially at temperatures for recrystallization annealing ($T \approx 1300$-$1500K$), the residual partial pressures of N_2 should be kept far below 10^{-5} mbar to avoid the formation of Nb_2N at the surface of the material.

In Figure 7b the N solubility in niobium at 2050 C and just below and above the corresponding melting points is plotted against the N_2 partial pressure. For a given N_2 pressure the N concentration in the melt is higher. This shows that during vacuum drop melting the reduction of N concentration is not only caused by the extremely low N solubility of the superheated melt but also by a redistribution between liquid and solid during solidification.

The Nb-O phase diagram is shown in Figure 8 (10, 17).

The O_2 equilibrium pressures are rather low compared with the pressure of volatile oxides NbO and NbO_2 and the equilibrium pressure of atomic oxygen. However, equilibrium data can be obtained from the temperature dependence of the terminal O solubility and the G° values of equilibrium oxides (10). It must be kept in mind that under conditions of thermodynamic equilibria which are established in a closed system the gas phase consists mainly of volatile NbO, Nb and less NbO_2, whereas O and O_2 are minor components which can be neglected.

The O solubility in solid a-Nb is given by the reaction (17)

$$O \text{ in } \alpha\text{-Nb(s)}: \log c_O = 1/2 \log p_{O_2} - 4.51 + 2020/T, \quad (1570 < T < 2270K), \tag{7}$$

with c_O in at.%, p_{O_2} in mbar and T in K.

The vapor pressures of the volatile oxides over O containing Nb were determined at (17)

$$NbO(g): \log p_{NbO} = \log c_{O \text{ in Nb}} + 9.12 - 28400/T, \quad (1870 < T < 2470K) \text{ and}$$

$$NbO_2(g): \log p_{NbO} = 2 \log c_{O \text{ in Nb}} + 7.12 - 24300/T, \quad (1870 < T < 2470K) \tag{8}$$

The solubility limit $c_{O,max}$ of O dissolved in Nb was determined as (10)

$$O \text{ in } \alpha\text{-Nb(s)}: \log c_{O,\,max} = 1.67 - 1680T, \quad (1070 < T < 1770K). \tag{9}$$

These relationships describe the thermodynamic behavior and constitution of the Nb-O system, but they give little information about the processes really occurring when niobium is annealed in a vacuum chamber where low O_2

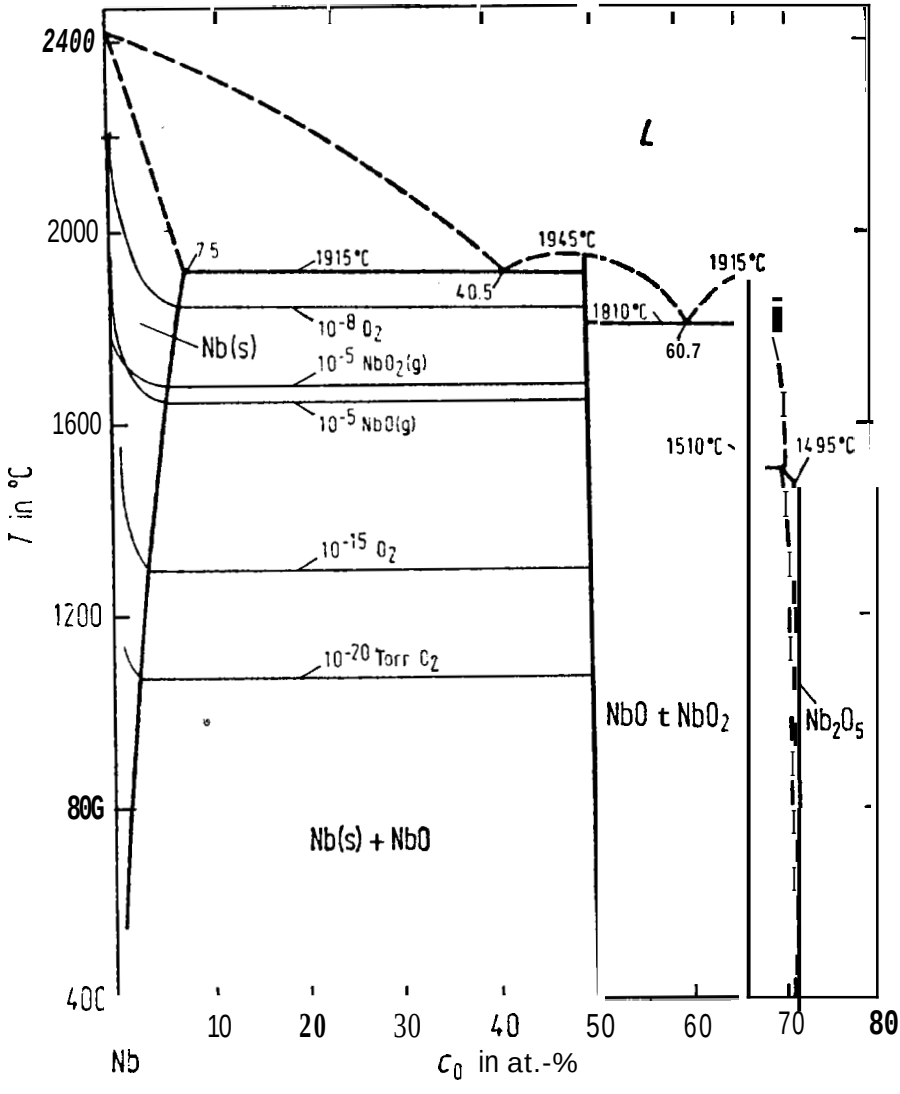

Figure 8. Nb–O System, T–c Diagram.

and H_2O partial pressures exist. Under these conditions at temperatures above 2000K both oxygen sorption and oxide evaporation from the surface are observed. The evaporating oxide condenses at the walls of the vacuum chamber. After long annealing times, the system finally reaches a steady state, in which the O concentration is a well defined function of the O_2 or H_2O pressures and temperature (18, 19).

The p-c isotherms for the steady states of niobium annealed in O_2 and H_2O are plotted logarithmically in Figures 9 and 10. The isotherms show a slope of 1, i.e. at constant temperature $c_O \alpha p_{O_2}$. The existence of the steady states is restricted to the region of the a-solid solution limited by the solvus and solidus lines (dotted and dashed lines in the upper part of the graphs). Furthermore, at low temperatures the steady state conditions cannot be realized any longer due to the negligible oxide evaporation which leads to a continuous oxygen sorption and oxidation. Only at very low O_2 or H_2O pressures are steady states still possible, but due to the extremely low reaction rates very long periods of attainment are necessary. At very high temperatures in the low pressure region the pure metal evaporation can exceed by far the oxide evaporation, see Figure 11, and thus the steady states are no more of importance. At higher temperatures and pressures O-containing melts are formed on the solid samples. Mass spectrometric investigations have shown (20, 21) that the monoxide NbO is the predominant evaporating species at lower concentrations and higher temperatures. The percentages of NbO are shown in Figures 9 and 10 by dot-dashed lines.

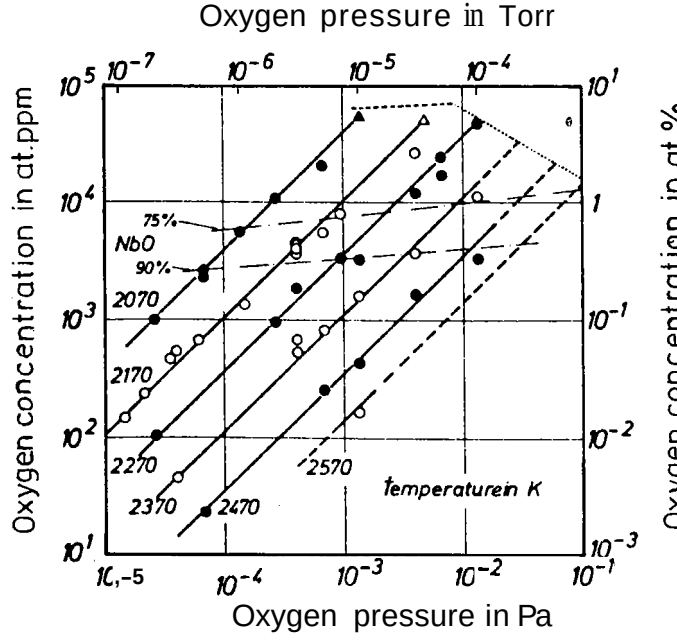

Figure 9. Steady States During Annealing of Nb in O_2 Atmosph.

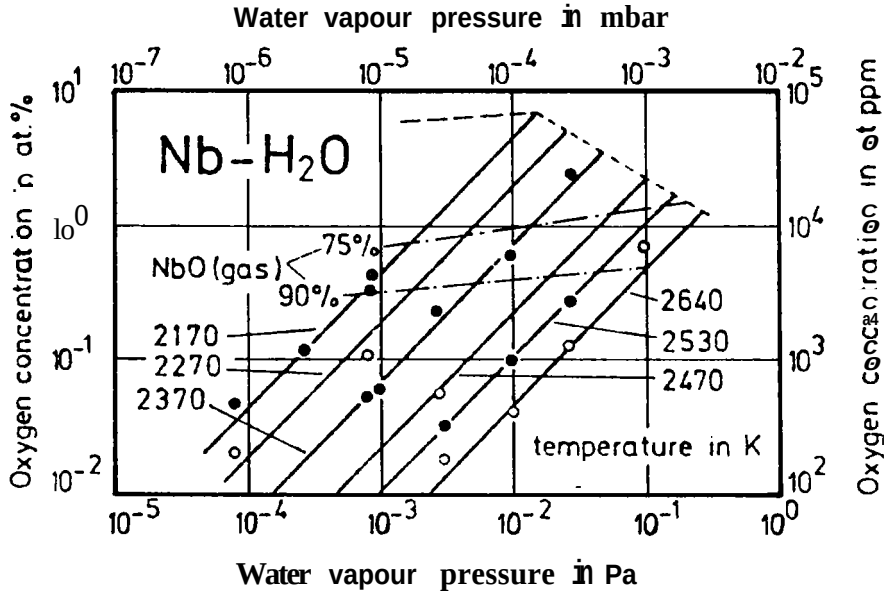

Figure 10. Steady States During Annealing of Nb in H_2O.

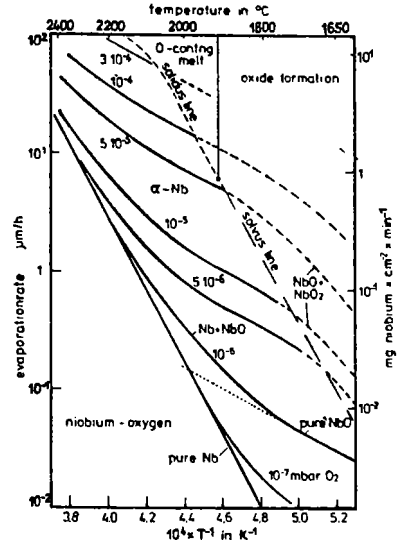

EVAPORATION RATES OF Nb in O_2 ATMOSPHERES AS FUNCTION OF 1/T; T-p RANGES FOR STEADY STATES

Figure 11. Evaporation Rates of Nb in O_2.

The steady state relations follow the equations

$$\text{Nb in } O_2\text{: } c_O = p_{O_2} \times 9.1 \times 10^{-8} \times \exp(-502000/RT),\ (2170 < T < 2540K) \quad (18)$$

and

$$\text{Nb in } H_2O\text{: } c_O = p_{H_2O} \times 1.47 \times 10^{-8} \times \exp(-480000/RT),\ (2170 < T < 2640K) \quad (19)$$

(10)

with c_O in at.%, p_{O_2} in mbar and R = 8.31 J/mol X K.

From these equations the minimum concentrations of O in Nb for a given O_2 pressure and temperature can be calculated. At low pressures and high temperatures the oxygen uptake of niobium proceeds via the partial steps (i) transport to the surface and absorption of O_2 molecules, (ii) dissociation and chemisorption, (iii) penetration and solution in the metal. Due to the energetics in the Nb-O system the reactions (i) and (iii) are reversible, while step (ii) is irreversible. Thus, the reaction of niobium with O_2 always results in absorption of O. The absorption rate is a function of pressure and temperature, i.e. $v_{abs} = f(p_{O_2}, T)$. The degassing takes place via the evaporation of volatile oxides and the degassing rate is a function of O concentration and temperature, i.e. $v_{deg} = f(c_O, T)$. The steady state is defined as $v_{abs} = v_{deg}$.

The marked difference between steady state and equilibri is also perceptible when the metal loss is regarded. In the steady state, besides the normal metal evaporation, a continuous metal loss occurs due to this oxide evaporation. The oxygen concentration of the metal keeps constant because for each absorbed O atom one NbO molecule desorbs.

The rate of O evaporation in the steady state is given by the relationship:

$$\text{Nb in } O_2\text{: } v_O = 2.22 \times 10^5 \times p_{O_2} \times \exp(-156200/RT),\ (2140 < T < 2370K) \quad (10)$$

and

$$\text{Nb in } H_2O\text{: } v_O = 5.8 \times 10^5 \times p_{H_2O} \times \exp(-154100/RT),\ (2140 < T < 2430K) \quad (11)$$

with v_O in $mgO/cm^2 \times min$, p in mbar and R = 8.31 J/mol X K.

From these equations the metal losses via oxide evaporation can be calculated for a given O_2 or H_2O pressure, temperature and time.

If the O_2 or H_2O pressures in the vacuum system are lower than the given O concentrations according to the equations for steady state conditions, then deoxidation takes place. In this case, the Nb losses via oxide evaporation directly correspond to the difference in O concentrations between the supersaturated solution and the steady state concentration for lower partial pressures. The kinetics of oxide evaporation are described below.

The Nb-C phase diagram is shown in Figure 12 (10). In the Nb-C system only the terminal solubility of the a-solid solution can be determined because reversible reactions between carbon-containing species of the gas phase and C dissolved in niobium are not existent.

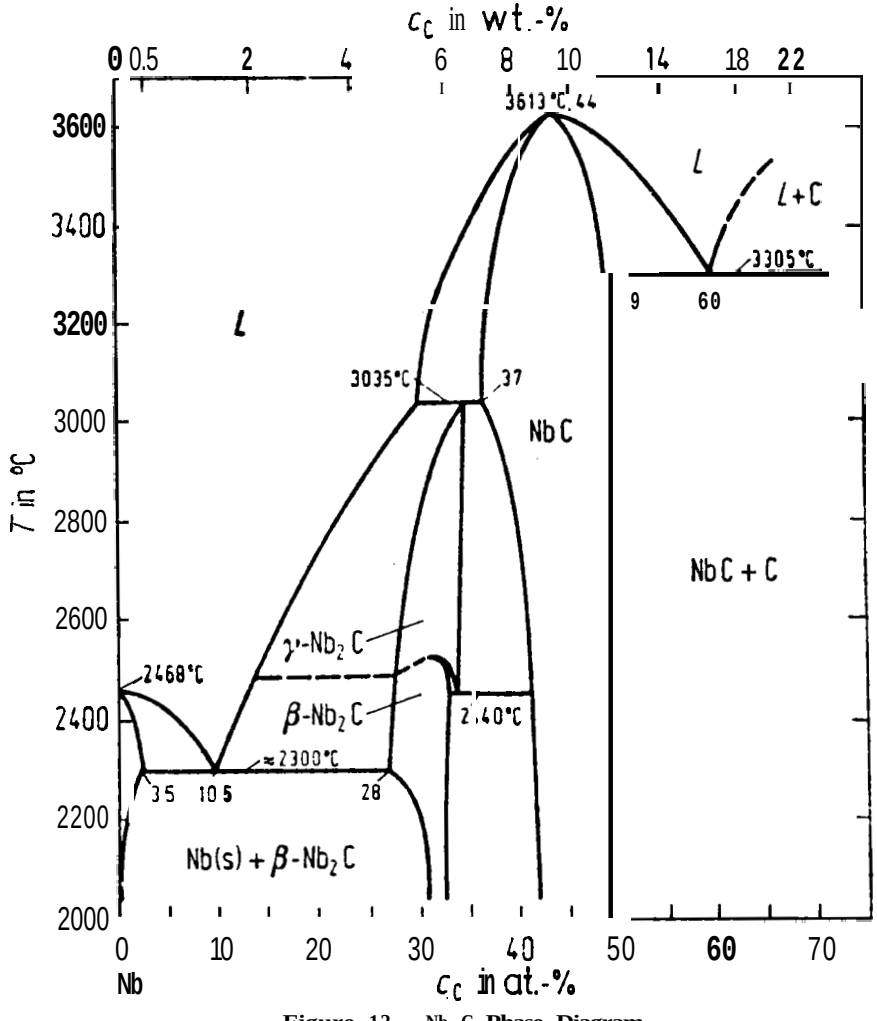

Figure 12. Nb–C Phase Diagram.

The solubility of C in niobium obeys the relationship (22)

$$C \text{ in } \alpha\text{-Nb: } \log c_{C,\,max} = 3.65 - 7600/T, \quad (1770 < T < 2470K). \tag{12}$$

When niobium is exposed to hydrocarbons, C_mH_n, at high temperatures, an irreversible carburization takes place. At high temperatures and low pressures molecular H_2 is liberated into the gas phase and C dissolves in niobium until the solid solubility limit is reached and the sample is converted to Nb_2C. The reaction kinetics of carburization of niobium in CH_4, C_2H_6, C_3H_8, C_4H_{10}, C_2H_4 and C_2H_2 are established (23).

During annealing of niobium in CO atmospheres, quasi-thermodynamic equilibria are established according to the reaction

$$(CO)_g \rightleftarrows [O]_{Nb} + [C]_{Nb} \tag{13}$$

The CO pressures over Nb-C-0 solid solutions are given by the expression (10)

$$O \text{ and } C \text{ in } \alpha\text{-Nb: } \log p_{CO} = \log c_C + \log c_O + 6.32 - 14700/T, \quad (1870 < T < 2170K) \tag{14}$$

In Figure 13 p-c isotherms are graphically shown on a logarithmic scale.

The CO equilibrium pressure over (C + O) - containing solid solution containing a few at.ppm of both interstitials at 2000 to 2600K is relatively high. Thus, the CO reaction can be used for removing carbon from niobium by a high vacuum treatment. For a given (C + O) concentration the equilibrium pressure of CO in the gas phase increases with increasing O concentration. Therefore, C can be removed by annealing the specimen in O_2 atmospheres.

Kinetics of Gas Reactions (Degassing)

The purification processes that occur during annealing and melting of niobium under vacuum conditions are volatilization of metallic impurities and degassing.

The degassing processes of niobium in the solid state have been investigated intensively (10). Only few results from theoretical studies and investigations of degassing liquid niobium exist (15, 24, 25). These results cannot be used for calculations because they cannot be transduced into generally valid equations. The main difference between solid and liquid degassing is that transport from bulk to surface in the solid state obeys the laws of diffusion, whereas in the liquid transport of impurities takes place via hydrodynamic flow. Therefore, the rates of degassing and volatilization processes are increased by orders of magnitude.

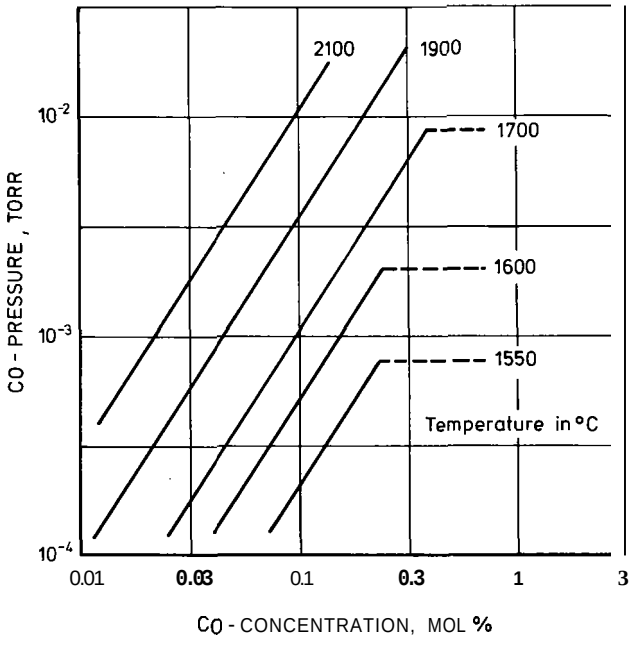

Figure 13, CO-Equilibrium Pressure of Nb-C-O Solid Solutions with C/o = 1.

The degassing mechanisms can be expected to be identical to those shown in Figure 4 for solid niobium; only the rate constants will be different. The increased evaporation rate of niobium itself and the higher solubility of gases in liquid niobium at a given partial presure (which makes superheating necessary) are detrimental to quantitative degassing. As could be shown very clearly for vanadium (25), it is impossible even under UHV conditions to reduce the nitrogen concentration below 1 at.%, because evaporation of metal competes with degassing. Similar limiting concentration in the ppm range can be expected for niobium.

The rate of volatilization of metallic impurities from liquid niobium is proportional to their partial pressures at the surface. The minimum concentration of metallic impurities is reached when the evaporation rates of the respective impurity and of niobium are equal.

Nitrogen. The time dependent change of N concentration is given by the expression

$$dc_N/dt = k_1 \times (T) \times P_{N_2}(T) - k_2 (T) \times c^2_N (T) \qquad (15)$$

If the rate of N uptake is neglected, a simple relation for N degassing for solid niobium is found (27)

$$v_N = 1.26 \times 10^{11} \times c^2_N \times \exp(-519000/RT) \qquad (16)$$

with v_N in *mg* X cm^{-2} X min^{-1}, *c* in at.% and R in J X mol^{-1} X K^{-1}.

Nitrogen degassing from niobium is shown in Figure 14 where for highest pumping speed S_{N_2} of the vacuum pumps the decrease of N concentration as a function of time is shown according to the first relation (15). For experimental conditions which can be realized easily (final nitrogen partial pressure 5×10^{-11} mbar, T= 2400K) for 10mm dia. rods, annealing times t > 1 week ate required to reach the ppm level and about 1 month is needed to achieve the thermodynamic equilibrium conditions.

Oxygen. Oxygen is liberated from niobium at temperatures T > 1900K in the form of the volatile oxides NbO and NbO_2. For O concentrations below 1 at.% the degassing via NbO is predominant. Besides, considerable losses of metal occur at higher temperatures and during deoxidation of liquid niobium. The deoxidation rate of solid niobium for thin samples (diffusion is not rate determining) is given by the relation (28)

$$v_\theta = 2.32 \times 10^{11} \times c_O \times \exp(543000/RT) \qquad (17)$$

with v_θ in mg X cm^{-2} min, c_O in at.% and R in J X mol^{-1} X K^{-1}.

Industrial Production (1, 4, 23, 30, 31, 78)

The main starting materials for consolidation ate powder, granulate or solid material from the reduction processes. Consolidation is achieved either by melting or sintering in high vacuum. Originally, the sintering technique was the only means of obtaining the high melting point metals in compact form. The high melting points and reactivity of niobium and tantalum have led to the development of tailor-made processes and equipment for melting. Above all, electron-beam melting (EBM) and arc melting in high

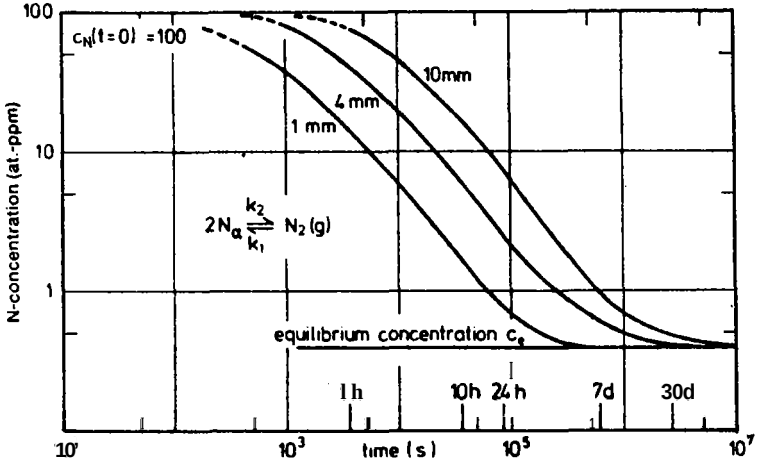

Figure 14. Degassing of N from nb Cylinders at 2400 K. $P_{N2e} = 5 \times 10^{-11}$ mbar and $S_{N2} = 10\lambda \cdot k_1(T)$.

vacuum have proved their value in melting, remelting and purifying these metals. For the first melt, powder, granulate and solid materials are pressed to form electrodes which are melted in vacuum. The material is then purified by repeatedly remelting under vacuum. EB zone melting or molten salt electrolysis can be used to produce metals of particularly high purity. A preliminary purification of the starting material by means of gas-metal reactions enhances the overall purification effect.

Electron–Beam Melting

As a result of the increasing demand for niobium and tantalum in the last few decades, the electron–beam furnace has been developed to a reliable, efficient apparatus for melting and purification. Electron guns serve as the energy sources.

The electron–beam, accelerated in a high potential, is focussed on to the metal to be melted, and nearly all the energy is converted into heat. Part of this energy is used to melt the electrode, part is used to keep the pool of metal liquid and the rest is lost to the surroundings. The whole volume of the furnace is under vacuum in order to:

- satisfy the particular requirements of the special metals,
- keep the energy losses in the electron–beam low, and
- to minimize wear and tear to the electron guns.

The reliability has been further increased by the development of tubular and transverse guns. The hot cathode, anode, focussing device and deflection system form a unit which can be evacuated separately from the main melting chamber. By means of this design, the cathode is protected from metal splashes, condensation and gas release. The different arrangements of electron guns have led to two alternative systems.

Figure 15 shows the vertical arrangement of tubular guns. The gun, Figure 16, produces a sharply bundled electron–beam with a round cross–section. The beam passes through the hole in the accelerating anode, is further focussed by electromagnetic lenses in the adjoining beam–directing tube and is then directed on to the melting material by an electromagnetic deflection system at the end of the gun.

A pressure difference can be maintained between the accelerating chamber and the melting chamber. Three or more guns are frequently combined to form a multiple gun system with integrated control. The beam directing tubes of the guns protrude only a short way into the melting chamber, Figure 15.

The other alternative, with transverse gun and magnetically deflected electron–beams, is shown in Figure 17. Under high potential, the cathode system produces a ribbon electron–beam. The electrons reach their velocity in the electric field between cathode and accelerating anode. An electro–magnet is positioned over the electron–beam source; its broad pol–plates reach to the edges of the mould. The ribbon–shaped beam enters the trans–verse magnetic field from below, and is turned by it on an almost semicircular path and directed on to the electrode and melt.

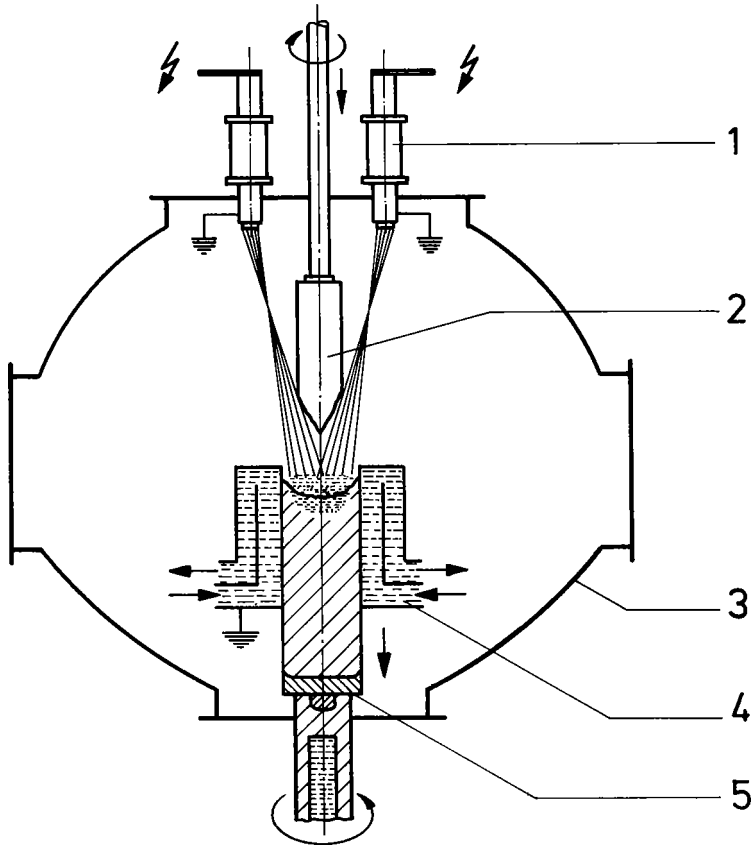

1 GUN
2 ELECTRODE
3 VACUUM CHAMBER
4 WATER COOLED MOULD
5 RETRACTABLE INGOT

Figure 15. Schematic Design of an E.B. – Furnace with Electron Guns.

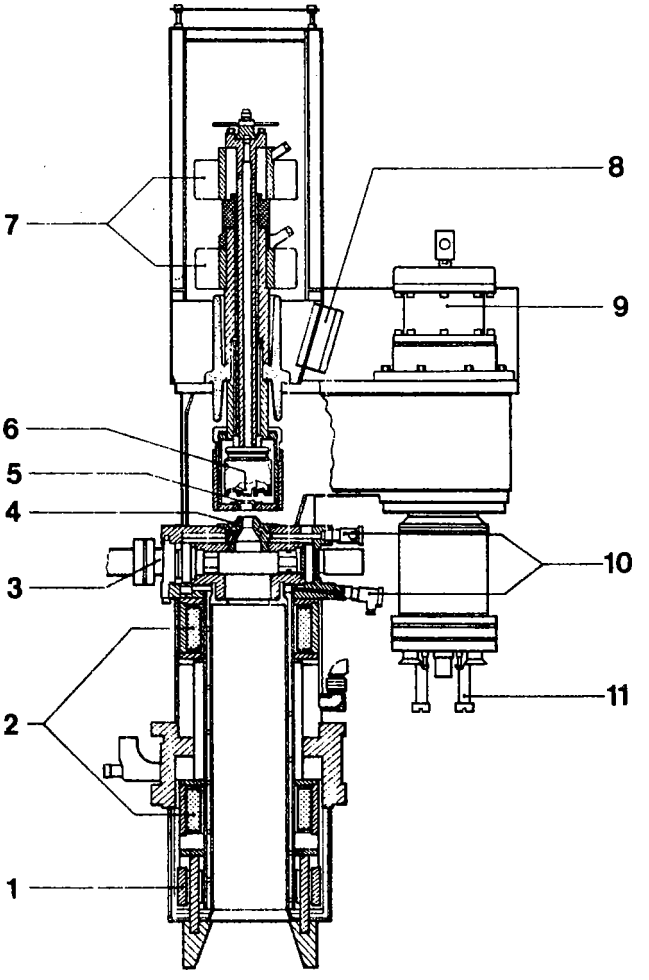

1 deflection coils
2 focussing lenses
3 gun valve
4 anode
5 Ta-block cathode
6 tungsten filament
7 cooling vanes
8 blower
9 vacuum valve
10 thermocouples
11 diffusion pump L 400 or turbo-molecular pump TMP 220

Figure 16. Tubular E.B. - Gun.

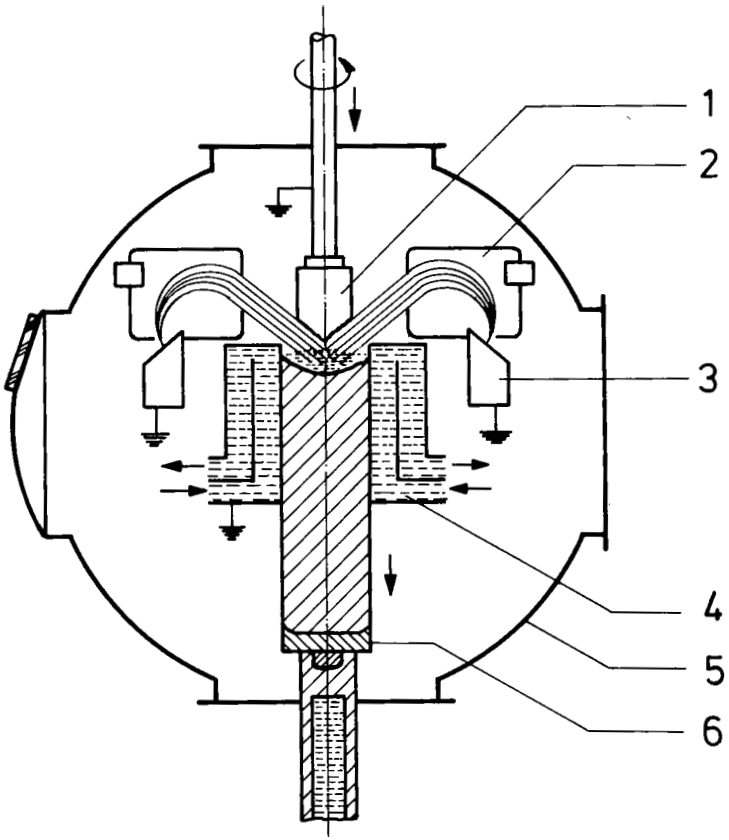

1 ELECTRODE
2 MAGNET
3 TRANSVERSE GUN
4 WATER COOLED MOULD
5 VACUUM CHAMBER
6 RETRACTABLE INGOT

Figure 17. Schematic Design of an E.B. - Furnace with Transverse Guns.

In both cases, Figures 15 and 17, the material drips down into a water-cooled mould. The solidified ingot is then withdrawn downwards on a base of the same material. The volatilization of impurities can be controlled both by regulating the superheating of the molten pool in the mould and by adjusting the rate of feed of the melting electrode. The melting electrodes are normally fed in vertically from above. A horizontal feed is also possible, which is used for preference during the first melt. The design capacity of the electron-beam furnace is determined largely by the melting point of the material to be melted and the diameters of electrode and mould. Figures 18 and 19 summarize the power requirements.

EBM is particular suited to the production of niobium ingots. Some examples are quoted below which support this statement. Figure 20 shows a furnace with a capacity of 300 kW which was built for purifying ATR niobium bars 80 x 80 x 800 mm, (ATR = aluminothermically reduced). With this unit, niobium ingots 150 mm diam x 1600 mm are produced by triple remelting. In the first melt, the material is fed in horizontally, and is fed in vertically in the second and third melts. The main process data are given in Table III. With the EB capacity of 300 kW and the limited pump capacity, the specific melting rate (kg/h) is significantly lower than in a 1500kW melting unit, as shown in Figure 21. In this second EB furnace, the power is delivered from 3 thyristor-controlled high voltage units of 500 kW at 30 kV each supplying two guns. During normal operation, each gun carries one sixth of the total power, which gives a good distribution of the EB power on the electrode and molten pool. This leads to very good values for degassing and purification and for material yield, Table IV. Operation is, however, also possible with only three guns. Each gun can carry up to 500 kW power.

Table III. Main Process and Productivity Data of the 300kW E.B. - Melting Furnace

Process Data *	Dim.	Melt # 1	Melt # 2	Melt # 3
Pressure	10^{-4} mbar	7	4	1.5
Ingot Melting Speed	kgh^{-1}	20	30	50
Ingot Melt/Prod. Time	h/h	12.7/14.2	8.5110	5/6.5
E.B. - Power	kW	172	240	250
Total Spec. Energy	kWh	12	10.2	6.5

Raw Material Niobium ATR-Ingot	ppm	Melt # 3 ppm
O_2	8000	150
N_2	300	40
H_2	50	5
C_2	500	60

Production of Niobium-Ingots 150mm Diam.
* Leybold-Heraeus

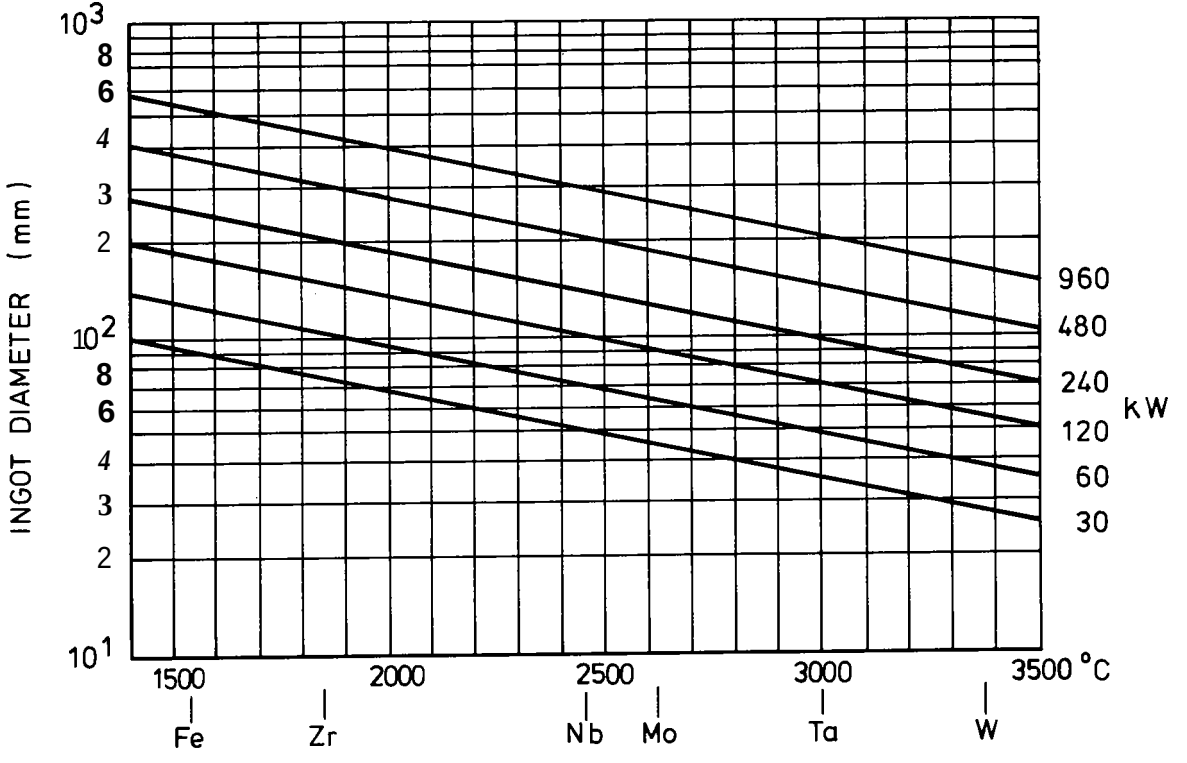

Figure 18. Power Requirements for Various Metals and Ingot Sizes.

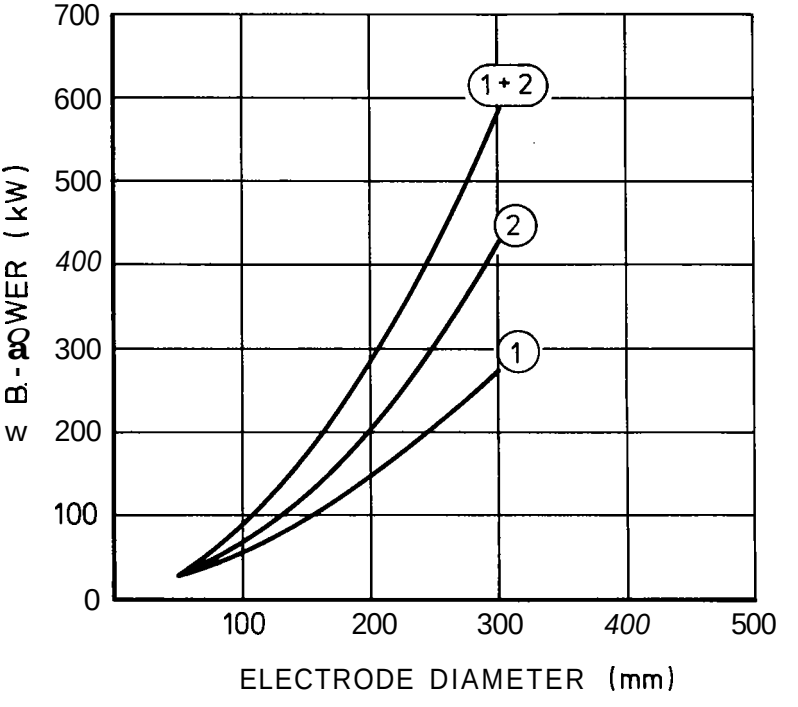

Figure 19. Electron Beam Power.

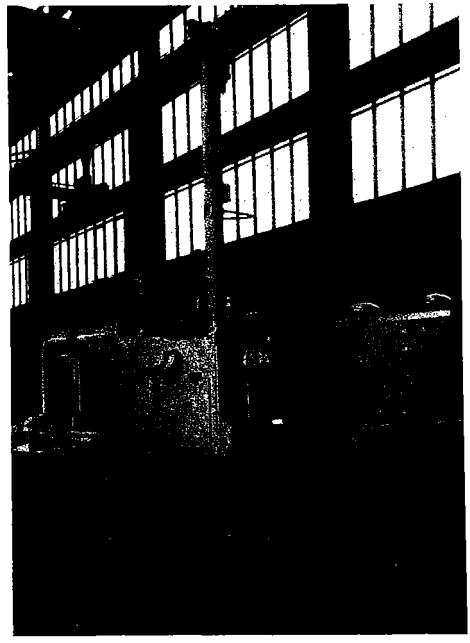

Figure 20. 300 kW EB - Furnace.

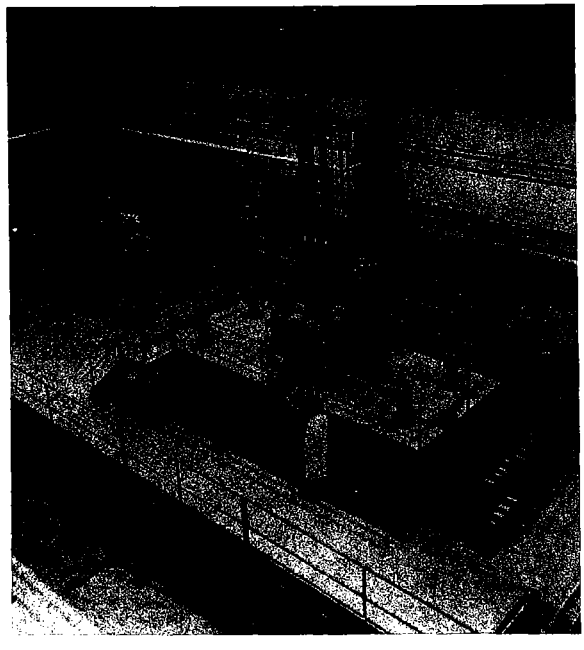

Figure 21. 1500 kW EB **- Furnace.**

Vacuum Arc–Melting

The vacuum arc furnace has, like the EB furnace, found application in melting reactive metals. The emphasis, however, lies in the melting of titanium and zirconium, whereas the EB furnace is used primarily for the more gas–sensitive metals such as niobium and tantalum.

In the vacuum arc furnace, an arc burns between the metal pool and the electrode. By repeated remelting, the homogeneity of the material, in particular, can be improved. Despite powerful pump systems and, therefore, a good vacuum, it is only possible to remove the most volatile impurities in the vacuum arc furnace. This results from the process parameters and, above all, from the small gap between electrode and metal pool and from the short time for which the metal is molten.

Sintering

The powder-metallurgically (PM) consolidated metals have a fine–grained structure which, in the case of the melted materials, can only be achieved by repeated deformation. The PM production process consists of numerous steps, Figure 22. The tough, ductile metals, such as tantalum and niobium, can be mechanically pulverized after charging with hydrogen during cooling from 950 C. After the hydriding treatment, the metals are crushed, ground, sieved and dehydrided in vacuum. The powder is then mechanically pressed to green compacts.

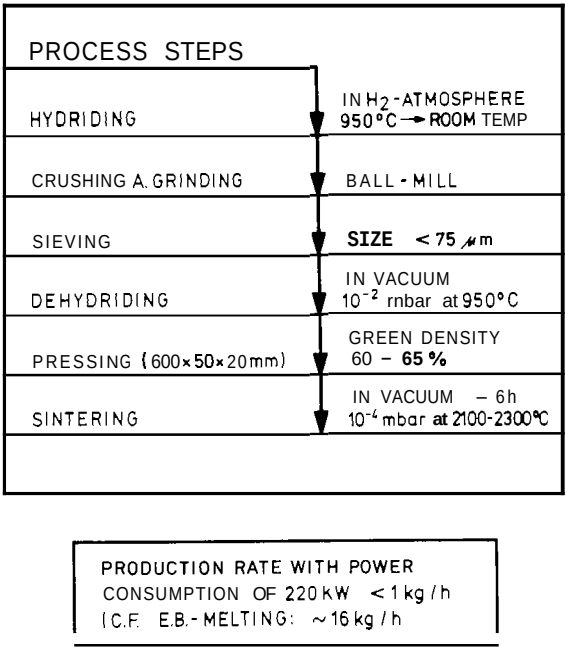

Figure 22. Process Steps for Niobium Sintering.

The temperatures at which sintering begins are dependent on the melting point of the metal and the nature of the powder: particle size and shape, surface condition and chemical purity are all important parameters. As a rule, metals are sintered at a temperature between 0.6 and 0.9 of the melting point with T in K. The sintering times are mainly in the order of several hours.

Sintering at excessively high temperatures leads to grain coarsening. The sintering is carried out in vacuum either by direct resistance heating or indirect heating. When compacts are sintered by direct resistance heating, Figure 23, the electrical contact is made via water-cooled copper clamps with brazed tungsten facings. The process is limited to regular-shaped bars and employs high currents at low voltage. The equipment requires expensive electrical installation and has a low energy efficiency. Sintering by direct resistance heating is still used, for example, for tantalum, and can also be applied to niobium. During vacuum sintering, a purification of the metals occurs, which leads to an improvement of the mechanical properties. The sintering temperature is increased in stages to permit evaporation of impurities and to prevent sudden gas release.

Fabrication

The production and fabrication of niobium is complicated by the fact that, at elevated temperatures, it reacts with all gases except for the inert gases, such as helium and argon. Titanium and zirconium react less strongly than tantalum and niobium. All heat treatments of niobium must be carried out in high vacuum or under a pure inert gas atmosphere. Even relatively small quantities of dissolved gases affect the mechanical properties. Pure niobium is ductile, and working is normally carried out at room temperature. The work hardening induced by this deformation is relieved by heat treating niobium between 950 and 1200 C in high vacuum or under a protective atmosphere. Larger deformation steps, such as forging, are carried out for preference at somewhat elevated temperatures up to about 600 C in air. Before an intermediate heat treatment, the surface scale of oxides and nitrides formed during warm rolling or forging must be removed to avoid oxygen and nitrogen diffusing into the bulk.

The rolling of niobium is similar to that of the other cold-ductile metals. Plate and thick sheet are normally rolled on two-high mills, thin sheet and strip are usually rolled on four-high mills and foils on multiple-roll mills. Foils are generally produced by package rolling.

In particular for niobium and tantalum, wire drawing is carried out in the pre-oxidized condition to avoid cold welding in the die. This oxidation treatment must be repeated after every few drawing operations. Figure 24 shows schematically the process steps in manufacturing mill products from ingot.

The niobium can be readily welded, although the reaction with atmospheric gases must be taken into account. Thus, welding is only possible under inert gas or in high vacuum. Also, alloying with steel or stainless alloys as a result of welding must be avoided. Here it is important to remember that the melting point of niobium is much higher than that of steel.

Niobium is machined with high speed steel or carbide tools. Cutting rate and angle correspond to those for stainless steels or aluminum.

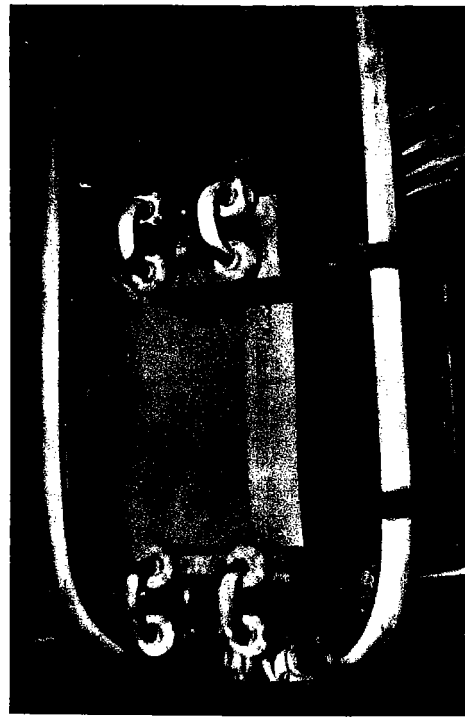

VIEW OF COMPACT IN SINTER UNIT

SINTERED BARS

Figure 23. Sintering by Direct Resistance Heating.

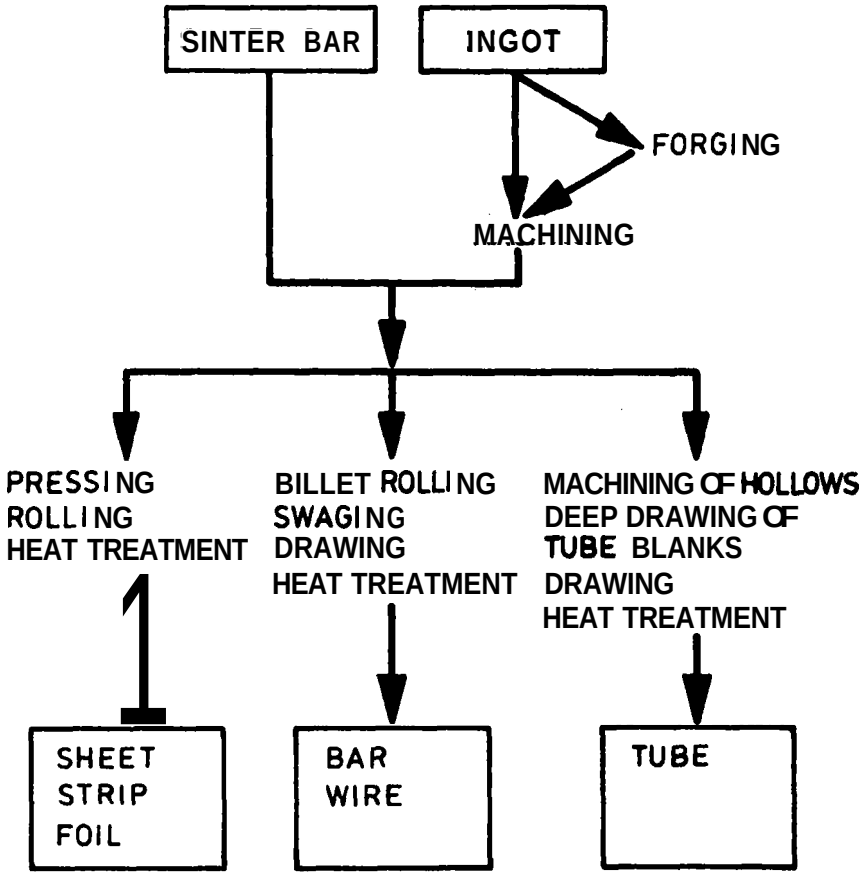

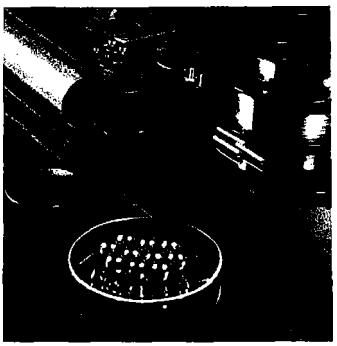

Figure *24.* **Niobium** Mill **Products.**

Processing of Different Starting Materials

Remarks about Commercial Qualities. A world-wide accepted specification for primary niobium does not exist to our knowledge. A comparison of qualities from different producers does not give any answer about representative qualities which are available on the market. In nearly all cases electron-beam melted (EBM) niobium is available.

Both the supply and production lines of niobium raw materials and also the reduction processes have shifted from pure columbite/tantalite to pyrochlore metallurgy, and as a consequence of this the technology has shifted from powder metallurgy to melting procedures. However, despite these changes, the problems of high-purity refining on an industrial scale remain unchanged, see Figure 1. On the other hand, due to the high efficiency of EBM for removal of volatile elements, the residual impurity level of commercial qualities is low and in most cases lower than certified by the supplier. Table V shows a comparison between the analytical results given by the supplier and the values that we determined in the MPI for an EBM-quality Nb. No typical analysis can be given, even if it is very often done for ultra-trace refining (32).

The results of improved analytical multi-element methods with high detection sensitivity show that:

1. The concentrations of all elements, except Ta and W, are much lower than certified; this is a question of the analytical methods and of the homogeneity of different lots of niobium.

2. Volatile metals are present at the lower ppm-level.

3. Ta and W show lower values than those common 10-15 years ago, but are still too high.

4. The analyses of interstitial elements agree well and the magnitude of the concentrations are tolerable for production on a commercial scale.

From these results, the conclusion can be drawn that other extraction, production or refining procedures must be applied to reduce Ta and W, and the non-metals to lowest possible concentrations. Furthermore, to describe the actual degree of purity, high detection sensitivity of analytical and physical methods are necessary. In this context standard reference samples of niobium for chemical analysis are required!

To demonstrate the effects of different starting materials on the melting and fabrication, a number of comparative tests have been carried out. The full programme is shown in Figure 25. The starting materials chosen were:

1. Granulate niobium produced by a hydride-dehydride process: Granule size 1-5mm, purity see Table VI.

2. Aluminothermically reduced bars with the dimensions 90 x 60 x 600 mm, purity see Table VII.

Table V. Comparison of Chemical Analyses of EBM-Niobium (Commercial Grade, TWCA) by Difference Methods in At.-PPM

Element/ Method	Producer's Analysis	SMS	IPAA	INAA	IRNAA
Al	< 70	40.0	--	--	0.09
Ti	< 76	< 1.0	0.7	--	0.002
Zr	< 100	2.9	1.6	—	--
Hf	< 25	2.9	--	1.0	0.3
V	< 35	< 0.9	1.0	ND	0.005
Ta	123	160.0	165	149	--
Cr	< 35	< 0.9	1.25	--	0.003
Mo	< 20	< 3.0	5.0	--	1.2
W	39	93.0	41.0	46	—
Fe	< 83	2.0	2.33	--	0.02
Ni	< 32	2.0	--	--	--
		KM	VHE	COMB	
H	~ 300		90		
C	< 230			36	
N	199	152	199		
O	522		556		

SMS = Spark Mass Spectrometry
IPAA/INAA = Instrumental Proton/Neutron Activation Analysis
IRNAA = Indicator Radionuclide Neutron Activation Analysis
KM = Kjeldahl Method
VHE = Vacuum Hot Extraction
COMB = Combusion Method

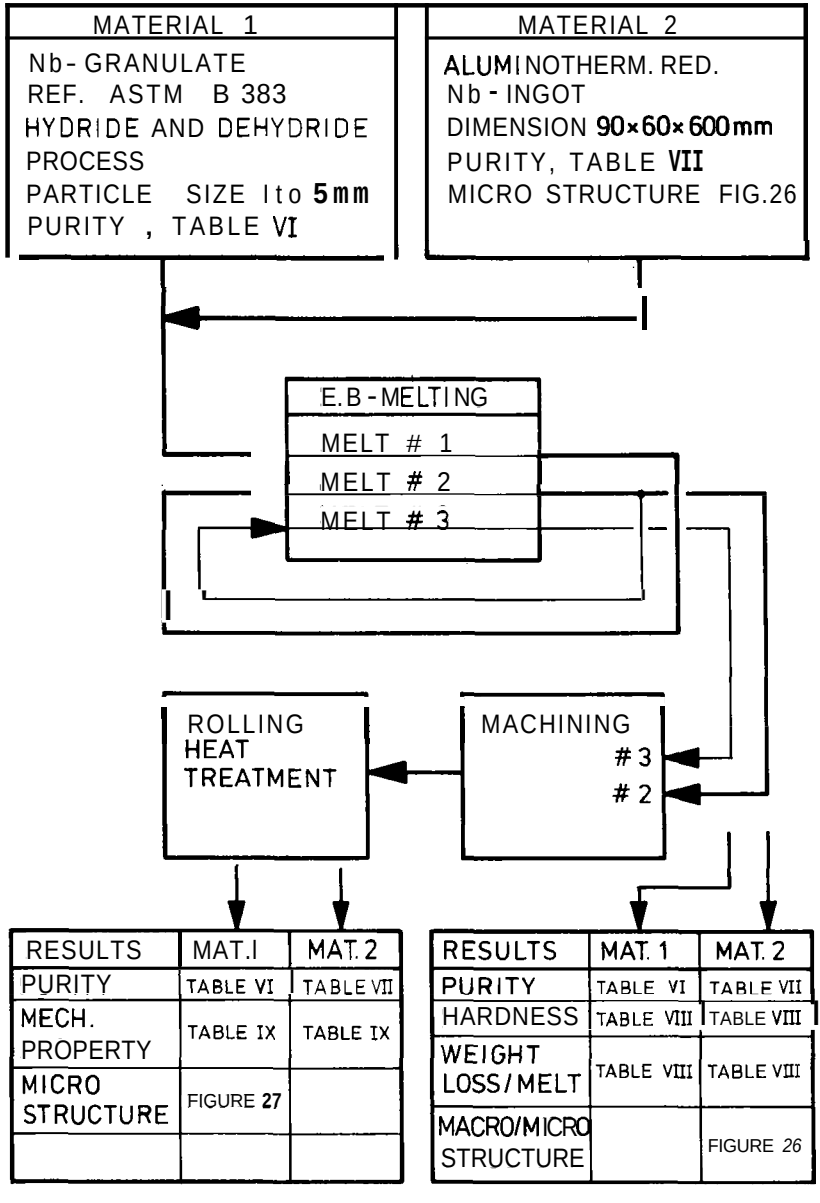

Figure 25. Program for Comparison of Mechanical Properties after E.B. - Refining and Fabrication.

Table VI. Effect of EBM on Purity and Hardness of Granulate Niobium

		Impurity Content, ppm		
		Melt		
Element	Granulate	# 1	# 2	1 mm sheet, 1h/1050 C
Mo	20	< 10	< 10	
Fe	15	12	< 10	
Ni	30	30	30	
Si	15	< 10	< 10	
Ti	< 10	< 10	< 10	
Zr	ND	< 10	ND	
Ta	< 150	< 150	< 150	
	50	50	50	
H	15-40			3.3
N	50-200			60
O	150-550			155
C				70
Hardness			59	65
(Ingot : HB 5/250 Sheet : HV 10)				

ND = None Detected (<< 10 ppm)

Table VII. Effect of EBM on Purity and Hardness of ATR-Niobium

		Impurity Content, ppm		
		Melt		
Element	ATR Ingots	# 1	# 3	1 mm sheet, 1h/1050 C
Mo	< 10	< 10	< 10	
Fe	400-1000	80	< 10	
Ni	10	< 10	< 10	
Al	0.5-1.4%	300	< 10	
Si	> 1000	250	50	
Ti	10	< 10	< 10	
Zr	ND	ND	ND	
Ta	1450	1450	1450	
W	40	40	40	
H	50	20	8	14
N	400-1000	95	30	80
O	2.3-4.5%	1800	130	180
C		70	40	
Hardness		117	51	64
(Ingot : HB 5/250 Sheet : HV 10)				

ND = None Detected (<< 10 ppm)

Electron Beam Melting

The melting was carried out in a production EB furnace with a power rating of 250 kW.

In the first melt, both the electrodes formed by pressing granulate and the ATR bars were fed in horizontally to the crucible and melted to an ingot of 100 or 125 mm diameter. The process data are summarized in Table VIII.

Particularly striking is the observation that with the ATR bars a melting loss of 26 percent occurred (first melt). The melting loss with the granulate was about 6.5 percent which can be regarded as an average value from previous experience. The high loss with the ATR bars can be explained by a combination of the evaporation of the very high oxygen content as NbO (2.5% oxygen evaporating as NbO would give a weight loss of about 17%), the evaporation of a large proportion of the aluminium and the high energy density and slow feed. A positive indication is that, after the first melt, the hardness values (HB) are already in some parts down to about 85.

In the second melt, the ingots were remelted vertically to a diameter of 100 or 125 mm. The process data are summarized in Table VIII. The melting loss of the bar-material was around 8.75 percent and that of the granulate was around 2 percent; these values can again be regarded as average values from practical experience.

A comparison of the quality shows that the HB-hardness'of the ATR niobium had already reached values between 68 and 76.

Table VIII. Main Process and Productivity Data of 250 kW E.B. - Melting Furnace

		Nb-Ingot Aluminotherm Red. Melt			Nb-Granulate Melt	
Process Data	Dim.	# 1	# 2	# 3	# 1	# 2
Ingot-Diameter	mm	125	125	150	100	100
Pressure	10^{-4} mbar	3	2	2	4	2
E.B. - Power	kW	130	150	220	85	120
Ingot Melt/Prod. Time	h/h	10.5	5	1	2.5	1.3
Ingot Melting Speed	kgh^{-1}	8.25	12.85	59	20	36
Weight Loss	%	26	8.75	1.40	6.5	2
Hardness HB 5/250 Head		159–185	68–76	56	95	62
Hardness HB 5/250 Bottom		76–94	68	52	90	58

In the third melt with the ATR starting material to a diameter of 150 mm, the hardness was further reduced by 15 - 20 points. This indicates a high purity level, which was confirmed by analysis, Tables VI and VII. Figure 26 shows the typical solidification structures of the ingots.

As a result of this remelting process, it can be stated that outstanding purity levels can be achieved by choice of appropriate melting parameters.

Fabrication to Mill Products

The ingots from the different starting materials were first turned to remove the surface and reduced to 12 mm thickness in individual reduction steps of 8 - 10 percent. The sheet blanks were then heat treated in vacuum. Subsequently, the sheets were rolled down to a thickness of 1 mm with individual reduction steps of 6 - 8 percent and again heat treated. The material for investigations was taken from this sheet.

The results of mechanical property determinations are shown in Table IX together with the gas contents of the sheet material. The values of mechanical property data are typical for niobium semi-finished products after recrystallization heat treatment. No significant difference was observed for niobium from granulate and ATR starting materials. Figure 27 shows the typical microstructure of the sheet after a heat treatment of 1h/1050 C.

Table IX. Mechanical Properties and Gasanalyses of 1 mm Sheet.

	Granulate	ATR
H (ppm)	3.3	14
N (ppm)	60	60
O (ppm)	155	180
C (ppm)	70	
Hardness HV:10 HV: 10	65	64
Proof Stress: Rp 0.2 (N/mm^2)	155	161
UTS: Rm (N/mm^2)	240	228
Elongation: A (%)	45	42

Mechanical properties and gas analyses of 1 mm sheet produced from granulate and ATR niobium (recrystallized 1h/1050 C).

Al-RICH
OXIDE PHASE

Nb-Al INTER-
METALLIC PHASE

STARTING MATERIAL
ALUMINOTHERM. RED. (ATR)

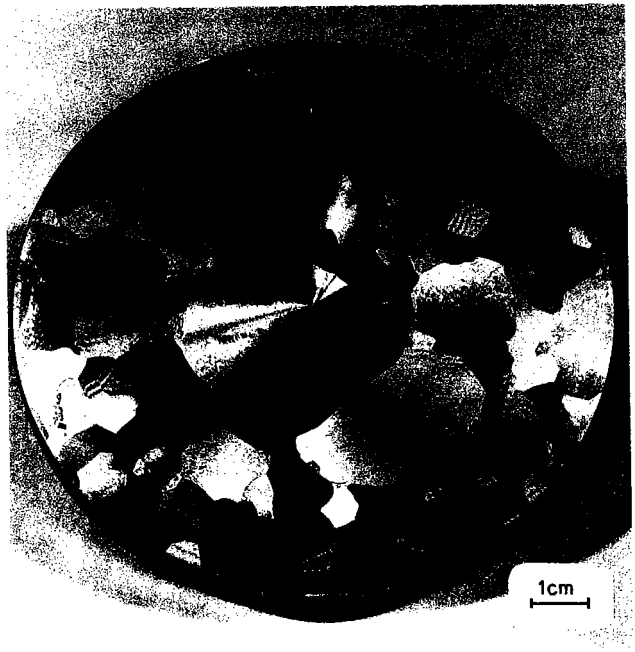

AFTER EB-MELTING

Figure 26. Macro/Micro Structure of Niobium (ATR).

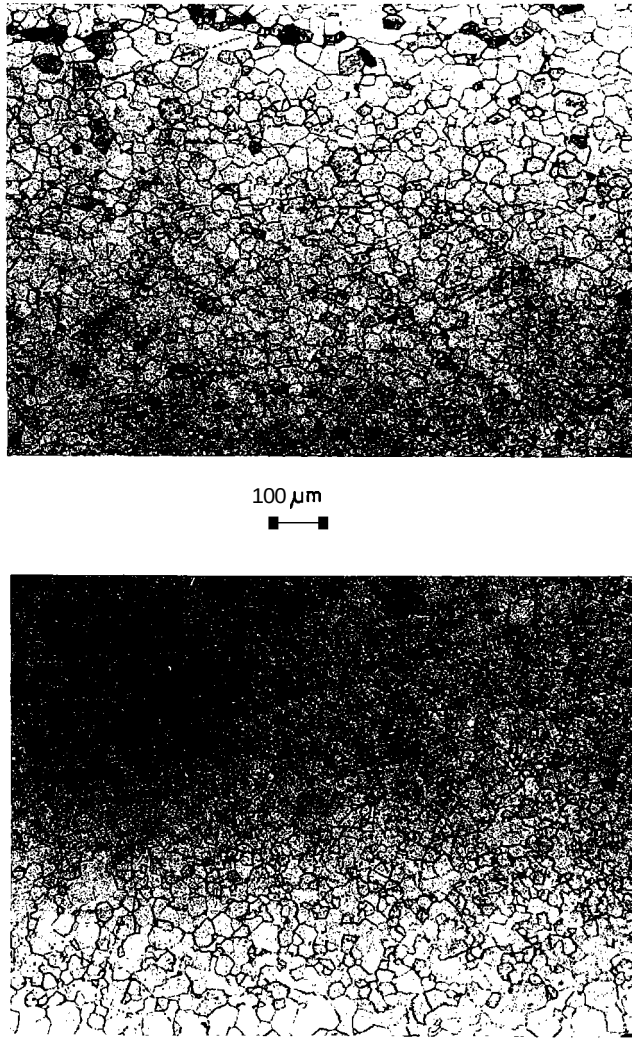

Figure 27. Micro-Structure of EBM – Niobium Sheet.

Special Purification Processes

Fundamental investigations of the electrodeposition of dense and coherent Nb-deposits from LiF-NaF-KF melts containing K_2NbF_7 at T ≈ 1000 K have been published by Senderoff and Mellors (33, 34). The authors emphasized that this electrolyte was not only suited for the production of coatings, but also that the material refined in this way showed improved mechanical properties and was extremely pure: Ta < 50, Fe < 480, Cr < 100, Cu < 146, Ni ~ 350, C – 7, O – 1200, and N < 30 at.-ppm.

Based on their results, we studied the optimum conditions for commercially available Nb, by which deposits of low metallic and non-metallic impurities could be produced (35). In a second series of experiments the homoepitactic growth on Nb single crystals was studied. By growing quasi single crystals the number of grain boundaries, and hence the inclusion of electrolyte, was reduced drastically. Nb rods prepared in this way can be zone melted directly, without any further treatment.

Electrolytic Refining

Reduction of impurity concentrations during electrolytic refining in molten salts depends mainly on the relative deposition potentials and concentrations of matrix and impurity atoms, and on the cathodic and anodic partial current densities of the species. In our experiments, 2.5 mole % K_2NbF_7 was added to the base electrolyte. The reduction steps of Nb^{5+} - ions, $Nb^{5+} \rightarrow Nb^{4+} \rightarrow Nb^{+} \rightarrow Nb°$, were found to be in agreement with the results of Senderoff and Mellors.

The cathodic current efficiency is strongly dependent on the Nb-valence. During the passage of current the mean valence decreases from n=5 according to the reactions

$$3Nb^{5+} + Nb^{+} = 4\ Nb^{4+}$$
$$4Nb^{5+} + Nb^{"} = 5\ Nb^{4+} \qquad (18)$$

and the current efficiency approaches 100 percent for n = 4. This reduction leads to an increase in niobium-concentration of the electrolyte.

The problem of valence is not restricted only to the beginning of operation. Oxidation of Nb-ions by oxygen or water traces introduced into the bath from leakage or from the electrodes leads to reduction of current efficiency and steady increase of Nb-ion concentration. Additionally, oxygen is picked up by Nb from the melt. Resides this oxidation of complexed Nb-ions, $4NbF_7^{3-} + O_2 = 4NbF_7^{2-} + 2\ O^{2-}$, formation of insoluble oxifluorides may occur, $NbF_7^{2-} + O^{2-} = NbOF_y^{(y-3)-} + (7-y)F^{-}$, which are incorporated in the Nb deposits. Corrosion of the Ni-crucible with formation of $NiNb_2O_6$ in the presence of Nb^{5+}-ions and O_2 can be observed.

The relation between the Ta concentration of cathodically deposited Nb and the Ta concentration of the electrolyte is shown in Figure 28. The upper curve shows the results of experiments using commercial quality Nb with 195 and 149 at. ppm Ta. The lower curve shows the results of a series of experiments in which traces of oxygen were carefully excluded. Ta contents of the electrolyte determined by chemical analysis and from the mass of dissolved anodes agree well with each other. From the results it can be deduced that for cathodic current densities $20 < i, < 50$ mA/cm^2 the Ta content of the deposits depends on:

1. the Ta concentration of the electrolyte and
2. the oxygen concentration.

However, the degree of purification does not depend on the Ta content of the anodes if the electrolyte is stirred by natural convection. The lowest Ta concentration of 0.05 at. ppm was achieved using commercial K_2NbF_7 with 300 at. ppm Ta as the Nb salt.

The minimum possible concentration of 0.02 at. -ppm Ta in Nb agrees fairly well with a value calculated via a redox reaction between Ta and Nb using published values for the standard potentials and the given ion concentrations (35).

The behavior of other metallic elements during electrolytic refining is shown in Table X. In column 1 the concentration of the starting materials (TWCA Nb) is given; in columns 2 and 3 the analyses of one or the content ranges of five samples purified separately by electrolysis, Nb–R–1, and EBFZM, Nb–R–2. In general, it can be stated that besides Ta, W and Mo concentrations can also be reduced. For other elements the low concentration level either remains unchanged or increases slightly, e.g. Fe and Al, due to contamination from structural materials.

Table X. Impurity Concentration* in Niobium.

Element	(TWCA Nb)[a]	Nb–R–1b	Nb–R–2[b]
Ta	83.0 ppm	0.05–3 ppm	0.05–3 ppm
W	3.8 ppm	1 - 30 ppb	1 - 50 ppb
Mo	1.2 ppm	96 ppb	75 ppb
Cr	3.0 ppb	6 - 28 ppb	17 - 44 ppt
Fe	26.0 ppb	1 - 3 ppm	3 - 11 ppb
co	85.0 ppt	0.3–2.5 ppb	6.3–30 ppt
cu	95.0 ppb	44 ppb	< 20 ppb
V	5.0 ppb	0.4 ppb	0.3 ppb
Ti	0.3 ppm	< 0.1 ppm	< 0.1 ppm
Al	90.0 ppb	110 ppb	20 ppb

* In atomic fraction, (a) averages from three determinations, (b) content ranges of separately purified samples.

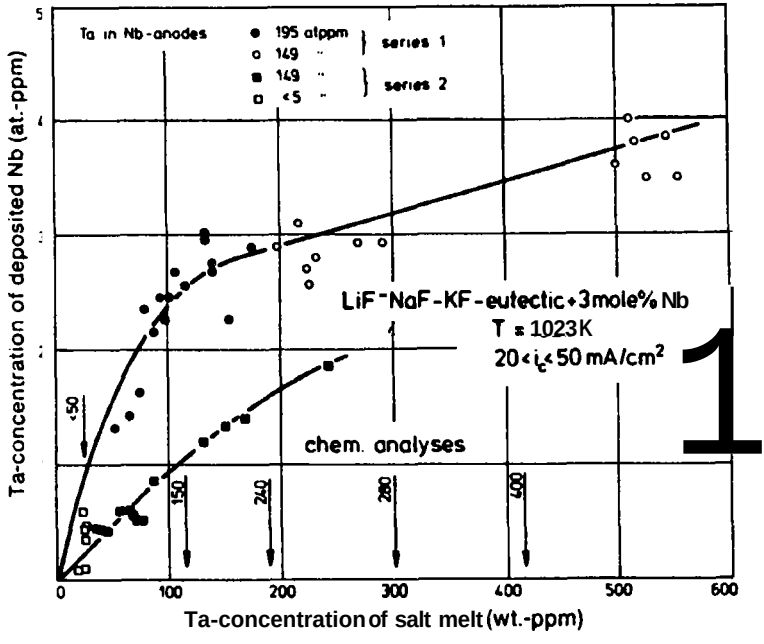

Figure 28. Nb–Purification by Electrolysis in Molten Salts.

Electrolytic Crystal Growth

The structure of electrolytic deposits on polycrystalline Nb samples showed that homoepitactic growth occurred on selected grains. Detailed investigations were therefore made on electrolytic growth of Nb single crystals. As an example, a cross–section of a crystal with < 110 > direction along the rod axis is shown in Figure 29. The results from deposition on cylindrical single crystals with < 100 >, < 110 > and < 111 > directions, and on single crystalline spheres can be summarized as follows:

- All crystals showed low–index faces and growth regions (100), (110), (111), and (112).

- Homoepitactic growth was observed for all surface orientations.

- Polycrystalline growth occurs if dislocations and low angle grain boundaries occur as a consequence of structural misfit, or if surfaces are contaminated by oxidation.

Electron Beam Float Zone Melting

As is well–known, zone refining has actually been found to be a minor part of the total purification effect of the EBFZM of niobium. The major purification mechanisms that occur are volatilization of metallic impurities and outgassing. Equilibrium distribution coefficients k_o determined from thermodynamic data and from experiments (36, 37) on niobium containing Ta and W show that, for volatile elements, k_o is less than 1.0, whereas the corresponding coefficients for Ta and W are k_{Ta} = 1.17-1.4 and k_W = 1.4-2.0.

Therefore, the redistribution of Ta and W at zoning speeds slow enough for the effective distribution coefficients to approach the equilibrium values ($\sim 10^{-4}$ cm/s) is opposed by an enrichment due to preferential evaporation of niobium.

The results shown in Table X designated as Nb-R, are obtained by EBFZM of the Nb-R-1 quality in vacuum $< 10^{-7}$ mbar with zoning speeds between 1.6 x 10^{-3} and 2.5 x 10^{-3} cm/s. Elements enriched during electrolysis, e.g. Fe, Al, Cr and Co evaporate quantitatively.

It must be emphasized here that with respect to metallic impurities in niobium, with the exception of Ta and W, many misinterpretations of the efficiency and the principal rules of zone refining have been published. This can be attributed to two simple explanations:

1. The detection limits of the applied analytical methods normally are too high, and

2. Contamination by residual metallic impurities from other experiments or structural materials was not considered.

As shown by Reed et al (38), severe contamination can occur by volatilization of impurities (oxides of Ta, W, and Hf) from the furnace walls by the radiant energy from the beam.

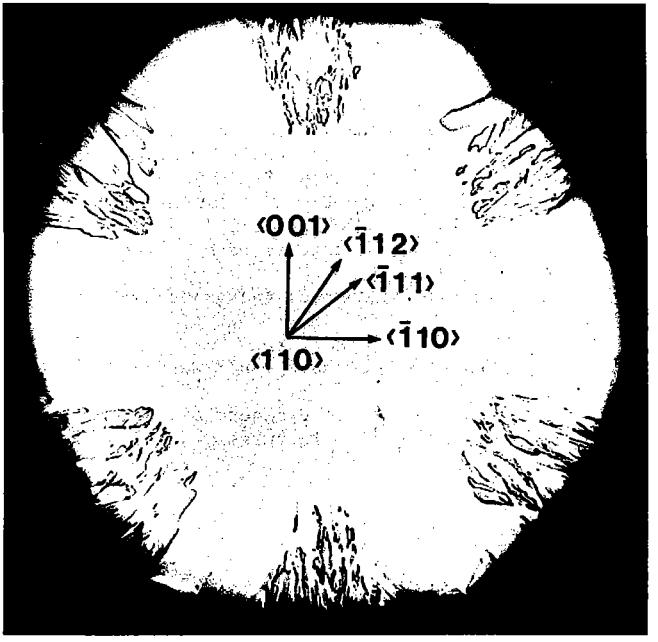

Figure 29. Cross-Section of Electrolytically Deposited Nb-Single Crystal.

On the other hand, the molten zone is probably protected from any interaction with the light molecules from the residual gases in the vacuum environment by a protective sheath of evaporating niobium atoms. Although the thermodynamic and kinetic conditions for degassing are more favorable for the molten zone than for the solid material, the lowest concentrations are observed after solid-state degassing. The final concentration of interstitial solid solution impurities, C, O, N and H will be affected by the degree of interaction between the heated solid rod and the residual gases. Normally, the partial pressures of the residual gasses are too high during zone melting ($> 10^{-8}$ mbar) to reduce the concentration of interstitials below the ppm level (39-41). Therefore, decarburization and degassing subsequent to zone melting are recommended. In a few cases, volatilization of metallic elements can occur even in the solid state, as was shown for Al and Zr dissolved in niobium (42, 43).

Analytical Techniques

General

In the scope of this condensed contribution it is impossible to review in detail the present state of the analytical determination of impurities dissolved in niobium. But, as can be deduced from the results of many publications on the purification of niobium, in general, the routine analytical methods used were not in general able to describe the real processes occuring during puification because the detection limits of the applied methods were too high. The preparation and optimization of industrial processes and application of pure niobium is closely connected with the possibility of the analytical description. Of central interest is the quantitative detection of very low concentrations, normally in the ppm and sub ppm-level, and the investigation of their local distribution. Thus, when the limits of capability of direct instrumental techniques (mass spectrometry, optical emission spectroscopy, activation analysis, direct application of atomic absorption spectrometry) are reached, traces of the elements of interest must be separated and/or enriched from the matrix before determination.

In addition, purification and analytical description of parameters which are characteristic for the processes must be treated as a unit because standard reference samples of high purity and definite composition are lacking and, conversely, extremely pure samples cannot be analyzed because reliable microtrace methods do not exist.

Since niobium is known to be a difficult matrix for trace analytical characterization, development and production of pure niobium have advanced more rapidly than characterization techniques. Therefore, as was already shown in section 3.5, Table V, by a comparison of chemical analyses of commercial grade EBM-niobium, the impurity level of several elements is lower by orders of magnitude than specified by the producer.

In collaboration with several European laboratories we are now able to analyze 25 of the most important residual elements in niobium (44), see Table XI.

This capability was reached only by an extensive multimethod concept for bulk analysis. As can be seen from Table XI, the detection limits depend on the impurities and methods and vary between 10^{-6} and 10^{-11} g/g niobium. If

possible, the instrumental activation analysis with thermal neutrons, protons or phonons is preferred because contamination can be reduced (45). For some elements, e.g. Cu, Cr, Fe, Co, Ni, Mn, Na or Ir, radiochemical tracer techniques with separation had to be developed to lower the detection limits (46-49). The concentrations of traces of C (50-52), O (54-55), H (50) and N (57, 58) are predominantly determined by improved classical methods.

Table XI. Analytical Characterization of High-Purity Niobium.

Impurities	Methods*	Power of Detection in μg/gNb
Ti, Cr	IPAA	0.05
Hf, Mo, V, Fe		0.1
Zr		0.4
W, Co, Cu, Sc, Se, Hg, Na	INAA	0.01 - 0.005
Ta		0.05
Co, Cr	IRNAA	0.0000 1
Al, Ti, V, Mo		0.006
Fe		0.005
Ni		01
Cu, Co, Cr, Fe, Co, Zn, Bi	IRPAA Electrolysis + OES/MIP	0.01 - 0.001
Si, Ni	Photometry	0.5
C	COMB (+ γ-AA) UHV-HE	0.5 (0.01) 0.01
N	Kjeldahl UHV-HE	0.5 0.02
O	VHE (γ-AA)	5 (0.02)
H	VHE	0.1 - 0.2

SMS - Spark Mass Spectrometry
IPAA/INAA - Instrumental Proton/Neutron Activation
IRNAA - Indicator Radionuclide Neutron Activation Analysis
KM - Kjeldahl Method
VHE - Vacuum Hot Extraction
COMB - Combustion Method

Analysis of Gases and Carbon

Because the gases and carbon have the strongest and most varied effects on the properties of niobium, and niobium-gas reactions play an important role during purification, fabrication and application, a short review of the present state of the analytical determination of the interstitials is given. In the contribution of M. W. Mallett (58) the state of the art up to 1974 is summarized. In this excellent survey, the classical methods are described in detail. The determination of the interstitials by activation analysis and recent results of standard techniques, as well as the problem of reference materials are thoroughly treated in the book edited by G. Kraft (59).

Hydrogen

Hydrogen determination has seen extensive development during the past decade. The high mobility of hydrogen in niobium, the high solubility and the formation of hydrides, the absorption of water vapor and the low rate of uptake at moderate temperatures, $T < 500$ K, complicate the definitive association of dates of fabrication with the real concentration. Niobium and tantalum usually contain 0.1 - 1 wt.ppm. Hot extraction methods are most commonly used for hydrogen determination. Sample weights of 5-20 g are preferable to minimize the effects of surface contamination. H is usually detected by thermal conductivity measurements with quite sufficient sensitivity in the order of a hundred wt. ppb.

To yield minimum surface contamination the samples are cleaned by etching and degassing (bath: 2 parts of HNO_3 (s.g. = 1.4) + 2 parts of HF (40%) + 1 part H_2O at room temperature for 1-2 min; washing 3 times with H_2O and 3 times with CH_3OH; drying with air at 60 C). The results of round robin tests (56) are prsented in Table XII.

The analyzed niobium sheet was produced powder metallurgically. The true H content of this material is probably less than 1 wt. ppm. Fusion and diffusion extraction methods yield comparable results, although the values for samples which were only washed are considerably higher. All samples which were exposed to the laboratory atmosphere for 8 weeks showed increased hydrogen contents and standard deviations. This was related to H uptake from acid vapors.

Nitrogen

The vacuum-fusion method has been applied to determine nitrogen along with oxygen in refractory metals (see oxygen). The detection limit for N in Nb ranges between 1 and 10 wt. ppm depending on the flux, samples and equipment (60, 61). For all vacuum fusion methods, the use of Pt-flux (Pt:Nb - 10:1) is recommended. Lower detection limits of a few hundred wt. ppb can be achieved by a UHV diffusion extraction method (53) or by an improved Kjeldahl method (60, 62). Figure 30 shows a comparison of the results of the Kjeldahl method, UHV diffusion extraction and electrical resistivity measurements of N-doped high-purity niobium rods. It is evident that N-concentrations down to 2-3 wt. ppm can be analyzed with the routine micro-Kjeldahl method. The most sensitive non-activation method is the UHV diffusion extraction with a detection limit below 0.1 wt. ppm. Niobium refined by EBM procedures from different producers usually contains 15-20 wt. ppm N. This is double the value which is analyzed for tantalum. The limiting factor seems to be the residual vacuum of the analytical methods for determination of nitrogen. The recommended surface treatment is given in the section on hydrogen.

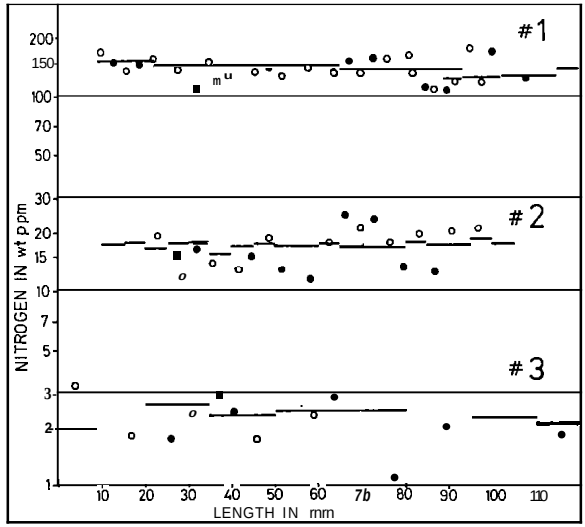

Figure 30. Comparison of Analytical Methods for N-Determination.

Oxygen

The vacuum fusion method in a graphite crucible using different fluxes, for example, Pt, Ni or Fe is the standard method now used. It was recently showed by simultaneously analyzing oxygen-doped samples of high purity and a commercial grade quality by vacuum hot extraction using the Pt flux technique, internal friction and residual resistivity measurements **(63),** Figure **31,** that the detection limit of vacuum extraction lies between **8** and 10 wt. ppm. Lower detection limits can be achieved by additional activation of the oxygen (52), e.g. photon activation (^{16}O (γ, n) ^{15}O, or by improved procedures of vacuum extraction (64), which allow a separation of surface oxygen from bulk concentrations by application of a mass spectrometer for detection.

For the oxygen determination in routine analyses, the vacuum hot extraction of oxygen using the Pt-flux sandwich-technique is recommended **(65).** Etched samples of **30-70** mg weight (see hydrogen) are packed into Pt-foil which is degassed at **1270K** in purified helium. The Pt/Nb ratio should be about 10/1. Because the sample and flux melt simultaneously, no reactions beween flux and the graphite crucible occur which might lead to a retarded alloying. According to this method, degassing at **2770K** occurs instantaneously and is finished after 30s. Contamination of the surface of the niobium samples occurs during storage in the laboratory atmosphere (see section "contamination"). Therefore, the samples must be analyzed immediately after the etching procedure.

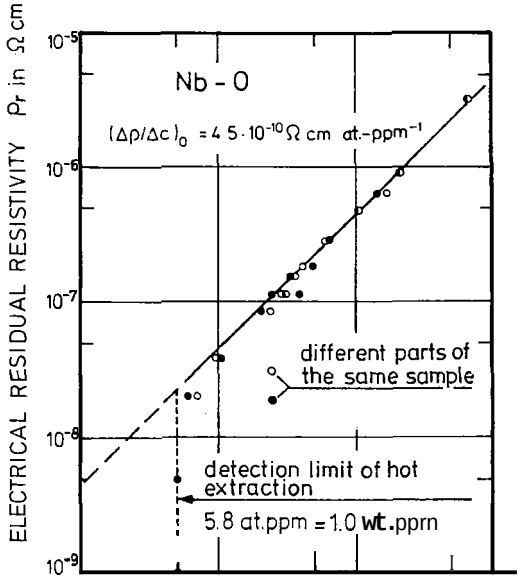

Figure 31. Oxygen Analysis of Doped Niobium by Vacuum Hot Extraction.

Carbon

The determination of carbon in the ppb-range by improved combustion methods is possible today. The combustion is performed by means of induction heating in high purity oxygen without additives. The CO_2 produced is determined after gas chromatographic separation using a relative conductometric method **(66)** or infrared absorption (58).

Another method for the determination is the UHV hot extraction of (C + O) containing niobium samples (53). The samples are degassed during levitation melting and the carbon monoxide which evolves is determined by a quadrupole mass spectrometer simultaneously with nitrogen. The method was checked by comparison of N- and CO doped niobium rods with the micro-Kjeldahl method, vacuum fusion and combustion of the sample (C) with oxygen and electrical resistivity measurements. The detection limit for (C + O) in Nb is about 50 wt. ppb, and for N in Nb **70** wt. ppb.

For routine analysis the combustion of niobium with purified oxygen in tube furnaces using Fe flux and Al_2O_3 - boats was found to be adequate. The CO_2 produced is determined by the conductometric method. In order to separate surface from bulk carbon the samples and flux are preburnt in argon containing traces of oxygen and after this in pure oxygen **(67).** Table **XIII** shows the results on commercial grade niobium which was analyzed using the combustion method with Fe-flux at 1400 C after "preburning" in Ar atmosphere. The detection limit is about 1 wt. ppm. For lower contents samples activated e.g. by photon-activation (^{12}C (γ, n) ^{11}C), must be used in order to reduce blanks (52).

Table XIII. Determination of C in Nb After Different Surface Treatments

rinsing in boiling toluol		
suface + bulk		128 (15 ; 6)
bulk		69 (3.5; 6)
rinsing in boiling toluol/ etching in $Hf/HNO_3/H_2O$ = 2/2/1		
bulk		49.6 (3.1; 12)

Determination of C in Nb at MPI - Stuttgart after different surface treatments. Combustion with Fe addition in O_2 after preburning in Ar. (100 mg Nb wire, 1 mm dia., W. C. Heraeus)

Contamination of Clean Surfaces with O, N and C

The behavior of clean Nb surfaces exposed to oxygen, air, or water vapor has been intensively studied using different methods (68-71) (Table XIV). Sorption experiments on metal films at low pressures using a volumetric method showed that (8-12) x 10^{15} molecules per cm^2 of O_2 and (1-3) x 10^{15} of N_2 are chemisorbed at ambient temperature (68). These values correspond to 0.4 $\mu g/cm^2$ O_2 and 0.05 $\mu g/cm^2$ N_2. Results from X-ray photo-electron spectroscopy (XPS) show that $Nb_2O_5/NbO_2/NbO$ layers are formed during storage in dry air as well as after electropolishing or etching. The formation of Nb_2O_5 layers with a final thickness of 6 nm (~ 0.45 $\mu g O_2/cm^2$) requires approximately 10 days for storage in air. A few at. % N_2 and several at. % C are incorporated into the oxide layer during growth. The mechanism is not yet well understood. Large quantities of water and hydrocarbons are absorbed into these oxide layers (69). Deuteron/proton activation analysis (^{16}O (d, p) ^{17}O) of etched and air-stored samples gives values ranging from 0.3 to 0.4 $\mu g O_2/cm^2$, whereas chemical analysis of similarly prepared Nb surfaces shows that ~ 0.9 $\mu g O_2/cm^2$, ~ 1.3 $\mu g C/cm^2$, and < 0.1 $\mu g N_2/cm^2$ are sorbed at the surface (70). These higher values can be explained by the additional analysis of those impurities which are absorbed on top of the oxide layers.

Table XIV. Sorption of Oxygen, Nitrogen, and Carbon on Clean Niobium Surfaces.

Analytical Method	Concentration, $\mu g/cm^2$		
	O	N	C
UHV-volumetry/films	0.4	0.05	---
XPS-polished sheet	0.45	~0.04	~0,2
160 (p,d) 170/sheet	0.3-0.4	---	---
Chemical analysis/foil	0.9	<0. 1	1.3

From these results the conclusion can be drawn that surface contamination with O, N, and C, and bulk solution of H to a greater or lesser extent, depending on the surface to volume ratio, must be tolerated. Surface protection layers serving as diffusion barriers or getters, e.g. Nb_2O_5 as a diffusion barrier for H or evaporated Si-Mo-Ti-Nb multi-layers can be prepared for special applications.

Analysis of Metallic Impurities

The routine analysis of metallic impurities in niobium leaves much to be desired. Traditional methods of chemical analysis, thoroughly reviewed by Porter (72) are now very rarely used - if used at all - because of their considerable expense and questionable reliability at trace impurity levels. For high accuracy analysis at levels below 5-50 ppm, a number of special techniques have been developed using spark mass spectrometry (77), proton or neutron activation, separation procedures using tracers, as described for example by Faix and Krivan (48).

These advanced techniques have served not only to permit the analysis of ultra-pure niobium, but also to demonstrate the technical irrelevance of a number of features of niobium specifications. Typical levels of the more volatile impurities have been shown to lie up to several orders of magnitude lower than the maximum values quoted in the ASTM specifications, see Table X. It therefore appears probable that the specifications bear more relevance to the detection limits of the routine analysis techniques for niobium than to the true impurity levels or to the normal requirements of the niobium user. However, the specifications satisfy most users' requirements and there appears as yet to be little motivation to change them.

For routine analysis of industrially produced niobium, manufactured and sold to conform to ASTM specifications, the main techniques used are:

- optical emission spectrometry (OES),
- atomic absorption spectrophotometry (AAS),
- atomic emission spectrometry (AES) and
- X-ray fluorescence.

At W. C. Heraeus, the first method is most commonly used. A high resolution spectrometer is employed which permits good line separation (0.125 nm/mm in the first order) and, thus, largely eliminates problems of interference from the complex niobium-spectrum. The sample is excited by means of a high intensity DC arc of 30 amperes.

The metallic sample is converted to oxide by exposure to air and, subsequently, oxygen at elevated temperature. Small quantities of additives are mixed with the oxide to stabilize the arc and to enhance volatilization. To increase accuracy of determination of elements which may be present in larger quantities (e.g., tantalum or tungsten), the sample is dissolved and the solution analyzed. The spectra, recorded on photographic plates, are evaluated first qualitatively and then photometrically to obtain a quantitative analysis.

The other analytical techniques normally used by W. C. Heraeus are AAS and AES. In both cases, the material is first dissolved in acid and the analysis performed on the solution.

When atoms are excited thermally or electrically, the energy taken up is re-emitted in the form of the emission spectrum. If the excitation is caused by light energy, the atoms only take up precisely defined energy components; here the absorption spectrum is observed.

The intensity of emission or absorption of light depends on the amount of energy released or absorbed and, thus, on the amount of the element taking part in the process. By measuring the light intensity via a photocell, the concentration of the element in the solution can be determined.

In the AAS devices, the irradiation source is a hollow-cathode lamp which emits a spectrum specific to a particular element. The excitation source in the AES devices, which simultaneously serves as irradiation source, is an electrically induced flame, i.e. plasma, containing ionized argon.

Applications

Niobium and some of its alloys (Nb-1% Zr, Ta-Nb, 50% Nb-50% Ti) have found a broad field of application either because of their particular physical properties or their corrosion resistance.

Therefore, a few special applications are briefly described below:

- niobium - 1 percent zirconium
as a material for the end caps in high-pressure sodium lamps

- 50 percent niobium - 50 percent titanium
as a superconducting material

- pure niobium
as the material for cavities in particle accelerators

- pure niobium and tantalum-niobium alloys
as materials in chemical plant

Niobium - 1 percent Zirconium

Since electric lighting was first introduced, the prime aim of research and development has been to increase the ouput of the light source. In view of the rising price and the shortage of energy, this aim is becoming ever more important.

The most successful development in this field over the last decade has been the high-pressure sodium lamp. Apart from the dense-sintered, translucent alumina ceramic, niobium or niobium - 1 percent zirconium is used in the discharge tube. Both materials are chemically resistant to the sodium vapor at a temperature of about 800 C. Furthermore, they have almost the same thermal expansion coefficient, so that the brazed joint between them is very reliable in service.

Therefore, this alloy is now the most commonly used material for the end caps in high-pressure sodium lamps. It is normally produced from niobium with an addition of zirconium.

The alloy components are mixed mechanically, pressed to melting electrodes and melting in the EB furnace. To achieve the necessary ingot homogeneity, it is essential that the alloy is double remelted. The alloy can be melted and fabricated in the same manner as pure niobium.

The material is very ductile at low temperatures. Thus, by means of suitable drawing processes, the final caps can be fabricated to precise tolerances directly from strip without intermediate heat treatment. Figure 32 shows various types of end caps.

It is estimated that the current annual production of the western world is around 20 million items for 10 million lamps. Niobium consumption is estimated at about 3–5 tonnes per year.

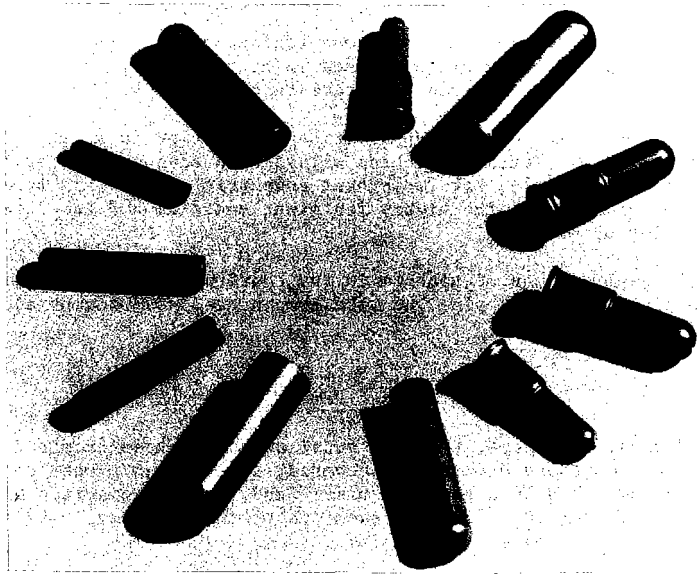

Figure 32. Various Types of End Caps. Niobium - 1% Zirconium.

Niobium - 50% Titanium (37)

The development of technical superconductors is largely associated with their application in magnetic coils for the production of high fields. With the development of ductile, superconducting, solid-solution alloys such as Nb-Zr and Nb-Ti, the development has reached a high technical standard. The construction and the choice of alloy are substantially determined by the application. Thus niobium with 44 percent to 52 percent titanium is a material which fulfills to a large extent the electrical, mechanical and fabricational requirements of a technical superconductor. Nb-Ti has excellent ductility and can be deformed to a reduction of well over 99.5 percent by rolling, drawing or, if necessary, by extrusion. Furthermore, it can be readily fabricated as a composite material with soft copper.

Niobium as a Cavity Material for Accelerators

In recent years, niobium has found application in accelerators, storage rings and RF-separators, as a result of its good superconducting properties.

All cavities have been made of pure niobium, either from solid material or sheet. "Reactor grade" material is used with a tantalum content less than 1000 ppm.

Niobium and Tantalum–Niobium Alloys for Chemical Engineering (11, 75, 76)

The metallic elements in groups IVa and Va show good corrosion resistance to aqueous solutions. The corrosion resistance is derived from the formation of a stable, dense, adherent oxide layer.

While tantalum, zirconium and titanium have already found a wide range of applications in chemical engineering, the corrosion resistance of niobium has still to be tested under service conditions.

Niobium shows, for example, very good resistance to nitric acid and, therefore, has a good chance of being used in nitric acid plant. However, a prerequisite is that the required long–term tests should be carried out.

A further potential area of application for niobium is as an alloying element for tantalum. Tantalum–niobium alloys show adequate corrosion resistance in, for example, hot 70 percent sulphuric acid. This broadens the range of materials between the highly resistant tantalum and the less resistant, high–alloy steels.

Possible applications of niobium in the construction of chemical equipment are in piping systems, pipe and tube components, measurement equipment, vessels and heat exchangers.

A Final Word

"Considering, therefore, that the metal which has been examined is so very different from those hitherto discovered, it appeared proper that it should be distinguished by a peculiar name: and, having consulted with several of the eminent and ingenious chemists of this country, I have been induced to give it the name of Columbium",

Charles Hatchett, 1802 (79).

References

1. G. L. Miller, Tantalum and Niobium, Butterworth Publication, Ltd., London (1959).

2. R. Kieffer and H. Rraun, Vanadium, Niobium, Tantalum, Springer Verlag, Heidelberg (1963).

3. A. N. Zelikman, O. E. Krein and G. V. Samsonov, Metallurgy of Rare Metals, Izdatel's Tvo Metallurgiy, Moscow (1964).

4. O. Winkler and R. Bakish, Vacuum Metallurgy, Elsevier Publishing Company, Amsterdam (1971).

5. W. Rockenbauer Chem.-Ing. Techn. 41 (1969) 159.

6. K. Schulze, J. of Metals 33 (1981) 33.

7. E. Fromm, Vakuum 21 (1972) 585.

8. J. D. Fast, Interaction of Metals and Gases, Vol. 2 Kinetics and Mechanisms; Mac Millan Press Ltd., London (1971).

9. J. Bigot, Le Niobium, in Monographies sur les Metaux de Haute Purete Tom II, G. Chaudron et O. Dimitrov (ed.); Masson, Paris (1977).

10. G. Hbrz and E. Fromm, "Niob", in Gase and Kohlenstoff in Metallen, E. Fromm and E. Gebhardt (ed.); Springer-Verlag, Berlin (1976).

11. D. Lupton, K. Schulze and F. Aldinger, this volume.

12. H. Wenzl and J. - M. Welter, "Properties and Preparation of Nb-H Interstital Alloys", Current Topics in Materials Science, Vol. I, E. Kaldis (ed.), North Holland Publishing Company, Amsterdam (1978), p. 603.

13. N. N. Kalinyuk and V. I. Lakomskiy, Izv. Akad. Nauk. SSSR Metally (1968) 28.

14. E. Gebhardt, E. Fromm and D. Jacob, Z. Metallkde. 55 (1964) 423.

15. W. Grünwald, F. Haessner and K. Schulze, J. of the Less-Common Met. 48 (1976) 325.

16. A. V. Revyakin and L. N. Kozina, Izv. Akad. Nauk SSSR Metally 48 (1976) 325.

17. E. Fromm, J. of the Less-Common Met. 14 (1968) 113.

18. K. Schulze and H. Jehn Z. Metallkde. 68 (1977) 654.

19. K. Schulze and H. Jehn, Proc. of 8th Vac. Congress, Cannes, (France), (1980), Vol. 11, Vacuum Technology and Vacuum Metallurgy, J. P. Langeron and L. Maurice (ed.).

20. I. Jupille and J. M. Michel, J. of the Less-Common Met 79 (1975) 17.

21. L. H. Rovner and A. Drowart, Report AF61 (052)-700 (1978).

22. E. Gebhardt, E. Fromm and U. Roy, Z. Metallkde. 57 (1966) 682.

23. E. Fromm and G. Hbrz, Int. Metals Reviews, Nos. 5 and 6 (1980) 269.

24. E. Fromm, Z. Metallkde. 56 (1965) 493.

25. G. V. Sokolova, Phys. Met. Metall. 47 (1980) 96.

26. G. Hbrz, Z. Metallkde. 62 (1971) 409, 416.

27. G. Hbrz, and E. Gebhardt, Z. Metallkde. 57 (1966) 737.

28. E. Gebhardt, E. Fromm and D. Jacob, Z. Metallkde. 55 (1964) 432.

29. R. Kieffer, G. Jangg, P. Ettmayer: Sondermetalle, Springer-Verlag, Heidelberg/Wien/New York (1971).

30. F. T. Sisco, E. Epremian, Columbium and Tantalum, John Wiley & Sons, Inc., New York, London (1963).

31. H. Stephan, W. Dietrich and A. Feuerstein, Statusbericht'uber die Elektronenstrahl-Hochleistungstechnologie,Leybold-Heraeus Hanau, Federal Republic of Germany (1981).

32. H. Y. Sohn, O. N. Carlson and J. T. Smith, Extractive Metallurgy of Retractory Metals, Proc. TMS-AIME. Session at 110th AIME Annual Meeting, Chicago, Feb. 22-26 (1981).

33. S. Senderoff and G. W. Mellors, J. Electrochem. Soc. 112 (1965) 266.

34. S. Senderoff and G. W. Mellors, J. Electrochem. Soc. 113 (1966) 66.

35. K. Schulze, E. Fromm et al in Reinststoffprobleme Bd. V, ed by M. Balarin; Akad, Verlag, Berlin (1977) 205.

36. L. Kuchar, P. Duzi and B. Wozniakova, Neue Hütte 21 (1976) 297.

37. R. E. Reed, J. Crystal Growth 19 (1973) 61.

38. R. E. Reed, C. W. Dean, R. E. McDonald and F. Emery, ORNL Report TM 2208 (1969)

39. R. E. Reed, J. Vac. Sci. Technol. 9 (1972) 1413.

40. D. C. Briggs and S. Saimoto, Jap. J. of Applied Physics 14 (1975) 113.

41. V. G. Glebovskii, V. V. Grimevitsh and B. M. Shipilevskii, Monokristally Tugoplavkich i Redkich Metallov, Splavov i Soedinenii, ed. by J. V. Tananae et al; 8th Moskva (1976) 14.

42. G. I. Nicolaev and N. V. Bodrov, Russ. J. of Phys-Chem. 52 (1978) 821.

43. H. Jehn and E. Olzi, High Temp.-High Pressures 12 (1980) 85.

44. G. Tölg, "Bulk and Distribution Analysis - Linked Strategy in Analytical Chemistry of High-Purity Materials". Proc. 5th Int. Symp. High-Purity Materials in Science and Technology, Vol. II, Dresden, GDR (1980) 53.

45. V. Krivan, Angew, Chem. 91 (1979) 132.

46. W. G. Faix, V. Krivan, and K. Schulze, Angew. Chem. Int. Ed. Engl. 19 (1980) 197.

47. W. G. Faix, J. W. Mitchell, and V. Krivan, J. Radioanal. Chem 53 (1979) 97.

48. W. G. Faix and V. Krivan, Z. Anal. Chem. 302 (1980) 269.

49. V. Krivan, Z. Anal. Chem. 290 (1978) 193.

50. E. Grallath, Z. Anal. Chem. 300 (1980) 97.

51. P. Schoch, E. Grallath, P. Tschöpel and G. Tölg, Z. Anal. Chem. 271 (1974) 12.

52. B. F. Schmitt and H. U. Fusban, Metall (1979) 1265.

53. M. Winterkorn, K. Schulze and G. Tölg, Mikrochimica Acta. Suppl. 7 (1977) 27.

54. K. Schulze, E. Grallath and M. Weller, in "Analysis of Non-Metals in Metals". G. Kraft (ed.), Walter de Gruyter Berlin (1981) p. 471.

55. R. Voigtmann and K. Friedrich, Mikrochimica Acta (1979) 115.

56. H. M. Ortner and D. Hirschfeld, Mikrochimica. Acta (1980) 475.

57. E. Grallath and G. Tblg, Mikrochimica Acta (1978) 547.

58. M. W. Mallett, in Determination of Gaseous Elements in Metals (L. M. Melnick, L. L. Lewis and B. D. Holt, ed.) John Wiley and Sons, New York (1974).

59. G. Kraft, (ed.), Analysis of Non-Metals in Metals, Walter de Gruyter, Berlin - New York (1981).

60. E. Grallath and G. Tblg, Mikrochimica Acta (1978) 547.

61. E. J. Merkle, J. W. Graab and W. F. Davis, Talanta 21 (1974) 1317.

62. W. Werner and G. Tblg, Z. Anal. Chem. 276 (1975) 103.

63. K. Schulze, E. Grallath and M. Weller, Z. Metallkde. 72 (1981) 439.

64. R. Voigtmann and K. Friedrich, Mikrochimica Acta (1979) 115.

65. K. Schulze and H. Jehn, Z. Metallkde. 68 (1977) 654.

66. P. Schoch, E. Grallath, P. Tschbpel and G. Tblg, Z. Anal. Chem 271 (1974) 12.

67. E. Grallath, F. Bhhler, A. Meyer and G. Tblg in "Analysis of Non-Metals in Metals". G. Kraft (ed.), Walter de Gruyter Berlin (1981) p. 395.

68. E. From and O. Mayer, Surface Science 74 (1978) 259.

69. M. Grundner and J. Halbritter, J. Appl. Phys. 51 (1980) 397.

70. K. Schulze and M. Bbrmann, unpublished results.

71. P. Boisot et al. Techn.-wiss. Bericht Nr. 76, Commission of the European Communities, Brussels (1972).

72. G. Porter, in "Columbium and Tantalum", ed. F. T. Sisco and E. Epemian, Wiley, New York, (1963) pp. 535-559.

73. Hans Hillmann, Tech. Supraleiter-Entwicklung u. Herstellung "Kerntechnik" 20 (1978) No. 6, 253-261.

74. W. Bauer, Fabrication of Niobium Cavities, Symposium Kernforschungszentrum Karlsruhe 1981.

75. F. Schreiber, Sondermetalle in der chemischen Verfahrenstechnik, Chemie-Technik 10 (1981) 203-206.

76. D. Lupton, W. Schiffmann, F. Schreiber and E. Heitz, 8th International Congress on Metallic Corrosion, Mainz 6.-11.9. 1981 Proceedings, Vol. II, pp. 1441-1446.

77. L. Radermacher and H. E. Beske, Kernforschungsanlage Julich Report JUL-1325 (1976).

78. S. Schiller, U. Heisig and S. Panzer, "Elektronenstrahltechnologie", Wissenschaftliche Verlagsgesellschaft, Stuttgart, (1977).

79. C. Hatchett, Phil. Trans. Royal Soc. London, Pt.I, (1802), p. 49.